Computer Modeling in
Engineering & Sciences

Tech Science Press

https://doi.org/10.32604/cmes.2026.084958

ARTICLE

Consensus Control Design for Heterogeneous Multi–Agent Systems in Vehicle Platooning Using an Event–Triggering Scheme

Muhammad Shamrooz Aslam[1,#], **Wen-Jer Chang**[2,*], **Hazrat Bilal**[3,*], **Vyacheslav Gulvanskii**[4], **Dmitrii Perevertaylo**[4], **Dmitrii Kaplun**[1,4,5], **Muhammad Hashim Bukhari**[6] and **Muhammad Aamir Aman**[7,*,#]

[1]School of Computer Science and Technology/School of Artificial Intelligence, China University of Mining and Technology, Xuzhou, China
[2]Department of Marine Engineering, National Taiwan Ocean University (NTOU), Keelung, Taiwan
[3]Center for AI Research (CAIR), University of Agder (UiA), Grimstad, Norway
[4]Intelligent Devices Institute, Saint Petersburg Electrotechnical University "LETI", Saint Petersburg, Russia
[5]Higher School of Artificial Intelligence Technologies, Peter the Great St. Petersburg Polytechnic University, Saint Petersburg, Russia
[6]Saudi Aramco LIP Star Building, Dhahran, Saudi Arabia
[7]School of Electrical Engineering, China University of Mining and Technology, Xuzhou, China

*Corresponding Authors: Wen-Jer Chang. Email: wjchang@mail.ntou.edu.tw; Hazrat Bilal. Email: hbilal@mail.ustc.edu.cn; Muhammad Aamir Aman. Email: aamiraman@cumt.edu.cn

#These authors contributed equally to this work

Received: 02 May 2026; Accepted: 12 August 2026; Published: 28 September 2026

ABSTRACT: In a multi-agent system, platoon vehicles receive a huge collection regarding autonomous models coordinating and their actions to improve traffic flow, lower fuel consumption, and boost safety. This paper examines the distributed consensus control problem for heterogeneous multi–agent systems (MASs) containing both first-order and second-order agents, under constrained network communication resources. Secondly, a novel event–triggered approach is proposed to tackle the problems of information transmission restrictions and bandwidth contention. Unlike conventional state-independent triggering methods, the proposed trigger condition depends on both the agent's own state update error and the information mismatches between neighboring agents, enabling a balanced trade–off between control performance and communication reduction. By ensuring that the transmission interval always exceeds one sampling period, the event-triggered technique significantly reduces network bandwidth usage. It determines the next transmission time for both position and velocity information. Thirdly, sufficient criteria for reaching asymptotic consensus are determined using Lyapunov stability theory and Kronecker product features. The trigger parameters and controller gains are obtained by solving linear matrix inequalities (LMIs). The distributed event–triggering mechanism and the consensus control protocol are integrated into a co-design framework. The effectiveness of the suggested strategy in conserving network resources without sacrificing system stability is validated by simulation results for a heterogeneous MAS with two second–order and two first–order agents, which show that all agent states converge to common values while the number of information transmissions is significantly reduced compared to periodic sampling.

KEYWORDS: Multi–agent system; resource constraints; event–triggering mechanism; consensus control

1 Introduction

Consensus control has been widely investigated in application domains such as distributed sensor networks [1], autonomous underwater vehicles [2], and cooperative unmanned ground vehicles [3]. In the power-system domain, coordinated protection and control strategies have also been studied to improve grid resilience under the high penetration of renewable energy resources [4]. The consensus problem, a key area of MASs research, seeks to create distributed protocols that, in spite of poor communication and dynamic uncertainty, motivate all agents to agree on specific quantities of interest, such as position, velocity, or heading angle. As a result, a lot of work has been done on this subject, and the literature has revealed many significant findings [5–7]. For example, Ref. [8] used linear consensus protocols to develop a theoretical foundation for average consensus under fixed and switching topologies. Ren and Beard [9] extended consensus analysis to multi–agent systems with dynamically changing directed interaction topologies and established convergence conditions based on directed spanning–tree connectivity. In order to minimize communication frequency while maintaining convergence guarantees, Ref. [10] presented distributed event–triggered consensus techniques. Adaptive consensus controllers for heterogeneous MASs with uncertain nonlinear dynamics were developed by [11]. Sampled–data consensus systems with time–varying sampling intervals and transmission delays were examined by [12]. For second–order MASs that are susceptible to input saturation, Ref. [13] developed fixed–time consensus methods. Consensus-based distributed secondary-control schemes have also been extensively reviewed for DC microgrids [14], demonstrating the broader applicability of graph-based coordination in networked power systems. However, such power-system-oriented methods do not directly address distributed event-triggered consensus co–design for heterogeneous vehicle platoons comprising mixed first-order and second-order agents. Moreover, existing studies on self-triggered consensus, communication-impaired formation control, and stochastic multi–agent systems [15–17] consider different agent dynamics, communication conditions, or control objectives. Therefore, a unified framework combining mixed-order heterogeneous dynamics, neighbor-dependent triggering, and simultaneous LMI–based design of controller gains and triggering matrices remains insufficiently investigated. In [18], researchers combine fixed–time reference generation with a self–structuring neural network that accounts for unknown nonlinear dynamics and external disturbances to create an event–triggered formation-control scheme for underactuated unmanned surface vessels. Conversely, Ref. [19] uses a mixed event-triggered mechanism to study completely distributed leader-following consensus for nonlinear fractional-order multi–agent systems, allowing coordinated behaviour through local information while lowering communication demand, because most existing approaches either concentrate on homogeneous agent dynamics or on first–order and second–order linear models.

The above–mentioned literature is all in the study of isomorphic multi–agent systems, all of which have the same dynamic characteristics. In the actual communication–limited multi–agent system, the competition for bandwidth of heterogeneous agents makes only some agents able to transmit data, and it is necessary to rationally schedule agents to reduce the transmission of information, save network resources, and ensure the optimization of network utilization and control performance. For example, Refs. [20,21] considered cooperative output regulation of heterogeneous linear multi–agent systems based on event–triggered control. In [20], a homogeneous MASs event–triggering mechanism is first established, followed by a new distributed event trigger control scheme is proposed for the internal reference model of each multi–agent to solve the problem of heterogeneous MAS cooperative output regulation. In [21] proposed a basic event–triggered control scheme for output regulation for multi–agent models. Based on this result, a distributed self–triggering control scheme is proposed, which can avoid continuous monitoring and measurement errors. Existing studies [21–24] investigate the consensus control problem of heterogeneous multi–agent systems based on event triggering mechanism under fixed and switching topology. Because the following elements are identified in Table 1 and an unfilled research gap is eliminated, the proposed multi–agent control, in contrast to the conventional event–triggered approaches, can offer a higher level of dependability and resilience.

Table 1: Summary of related literature on fault–tolerant and event–triggered control for nonlinear systems.

Ref.	Model Type	Controller Type	NCS	Optimization Method
[8]	H–MAS	LC protocols	Periodic sampling	Algebraic graph theory
[9]	First–order H–MAS	Linear consensus protocol	Switch Directed topology	Direct spanning tree analysis
[10]	H–MAS	DC controllers	ET (first generation)	Lyapunov–based Approach
[11]	H–MAS	AC controllers	Time–triggered	Adaptive control
[12]	Direct–MAS	Consensus controllers	ET	ARE–based design
[13]	Second–order MAS	FC protocols	Time–triggered	Fixed–time stability
[14]	DC microgrid MAS	Consensus-based distributed control	Distributed neighbor communication	Review of consensus control strategies
[15]	General–MAS	Self-tuning dynamic ET controller	Dynamic ET & self–triggered	Lyapunov and algebraic graph analysis
[16,17]	Networked USV MAS	Game & SSNN-based formation controllers	Packet-loss-aware ET communication	Noncooperative & SSNN fixed design
[18,19]	N–MAS	Adaptive distributed consensus controllers	Predefined-time with ET mechanisms	Backstepping & Lyapunov analysis
[20]	H–MAS	CR	ET	Internal model principle
[21]	H–MAS	D-SF control	SF	Output regulation theory
[22–24]	H–MAS	Consensus controllers	ET	Lyapunov + LMI
[25]	A–MAS	VAR-Control	×	Data imputation
[26]	H–MAS	Voltage–Control	×	Genetic algorithm
[27,28]	H–MAS	CR	ET	Internal model + ET
[29,30]	General NCS	×	Conventional ET	No co–design
[31]	Vehicle platoon	Absorption control	×	Parameter tuning
[32]	MAS (Delays)	Leader–follower	Time–triggered	LMI + Lyapunov
Our Method	**N–MAS**	**CC**	**Distributed controller**	**Co–design (LMIs)**

Note: ET: Event–Triggered. H–MAS: Homogeneous Multi–agent System. LMI: Linear Matrix Inequality. NCS: Networked Control Scheme. LC: Linear Consensus. DC: Distributed Consensus. AC: Adaptive Consensus. FC: Fixed Consensus. CR: Cooperative Regulation. CC: Consensus Controller.

This research studies the consensus control problem for heterogeneous multi-agent systems containing both second–order and first–order agents, based on a new distributed event–triggering mechanism. Using the stability principle of the Kronecker product and Lyapunov's function, sufficient conditions for consistency are given. The transmission strategy based on this trigger mechanism has the following improvements compared with the existing literature:

Although event-triggered consensus for MASs has been documented [10,21,24], the majority of current findings either examine first-order and second-order systems independently or concentrate on **homogeneous** agent dynamics. Furthermore, traditional event-triggering conditions ignore neighbor information and rely simply on the state error of each agent. On the other hand, this work's **novel contributions** are:

1. This paper studies the consensus control problem of second–order and first-order heterogeneous multi–agent systems, based on a new distributed event–triggering mechanism. The authors propose a co–design method where the stability conditions (using Lyapunov–Krasovskii with Kronecker product) are solved simultaneously to obtain both the controller gains $\left(\mathcal{K}_1, \mathcal{K}_2\right)$ and the trigger matrices $\left(\rho_1, \rho_2, \rho_3\right)$ using LMI tools.
2. Unlike traditional event–triggered mechanisms that rely only on the agent's own state error (e.g., Refs. [19,24] mentioned in the References), the proposed trigger condition considers both the agent's own information update error and the error between its current information and that of its neighbors.
3. The proposed strategy defines separate event–triggering functions for position and velocity, allowing independent distributed transmission of position and velocity information. The strategy determines the next transmission time for each type of information. In contrast, the agent's own state error is employed in [19,24]. By including neighbor errors, the trigger condition directly reflects the global consensus error, leading to fewer unnecessary transmissions during transients.
4. The trigger mechanism contains multiple tunable parameters $\left(\xi_1, \xi_2, \zeta_1, \zeta_2, \zeta_3\right)$, and matrices $\left(\sigma_1, \sigma_2, \sigma_3\right)$, allowing researchers to adjust the information transmission times and controller gain according to actual task requirements.
5. While many existing studies focus on homogeneous systems with identical agent dynamics, our research explicitly addresses a heterogeneous multi-agent system comprising both first-order and second–order agents within a unified event-triggered control framework. This mechanism is designed to automatically reduce transmissions once the system reaches consensus. Specifically, when (μ_{xi}) and (μ_{vi}) (position/velocity update status) tend to zero (i.e., consensus is achieved), the system transmits information less frequently to maintain the achieved state.

2 Related Work

Due to its numerous applications in distributed sensor models, power sector, wireless communication, and cooperative unmanned ground vehicles, the consensus control problem for multi–agent systems has attracted a lot of attention in the last ten years [25,26]. Early research, mostly focused on homogeneous multi-agent systems, established theoretical foundations for average consensus under fixed and switching topologies by *Olfati–Saber and Murray*. Later, *Ren* and *Beard* [9], extended the consensus analysis to dynamically changing directed interaction topologies and derived convergence conditions based on directed spanning-tree connectivity. Realizing that network communication resources are inherently limited, researchers such as *Dimarogonas* and *Johansson* developed event–triggered control algorithms to reduce transmission frequency while maintaining convergence guarantees. However, these early event-triggered methods mostly relied on each agent's own state error as the triggering condition, without considering interactions with neighboring agents. Researchers have studied cooperative output regulation using event–triggered control based on internal reference models for heterogeneous multi–agent systems [27,28], where agents may have different dynamics (e.g., mixed first–order and second–order dynamics). They have also developed distributed self–triggering schemes that do not require continuous monitoring. Although consensus control for heterogeneous systems under fixed and switching topologies has been studied more recently, the majority of current methods either tackle first–order and second–order linear models independently or concentrate on homogeneous agent dynamics. The relationship between an agent and its neighbors, which contains important information about the consensus status of the entire system, is usually ignored by conventional event–triggered mechanisms, which define trigger conditions only based on the difference between an agent's current state and its last transmitted state. Additionally, most studies treat controller design and communication scheduling as distinct problems, resulting in suboptimal trade–offs between control performance and resource utilization [29,30]. This is because the literature currently in publication lacks systematic co–design frameworks that simultaneously optimize controller gains and event–trigger parameters. The present study fills these gaps by proposing a novel event–triggered consensus control strategy that incorporates neighbor information into trigger conditions, creates independent event functions for position and velocity, and offers a co–design framework for simultaneously determining trigger parameters and controller gains using linear matrix inequalities. Thus, following are the main innovations of this paper: (i) a neighbor-information-dependent event trigger for mixed first-order/second-order heterogeneous MASs; (ii) independent event functions for position and velocity with guaranteed minimum transmission intervals via parameters ξ_1, ξ_2; (iii) a co-design LMI framework that simultaneously solves for trigger matrices ρ_1, ρ_2, ρ_3 and controller gains $\mathcal{K}_1, \mathcal{K}_2$; and (iv) automatic reduction of transmissions as consensus because the trigger condition uses μ_{xi}, μ_{vi} that disappear at consensus. By including neighbor errors, the trigger condition directly reflects the global consensus error, leading to fewer unnecessary transmissions during transients.

3 The Requirement of Vehicle Platoon Control Design

This research investigates a group of m vehicles traveling in a single–file formation. The vehicles are numbered sequentially from $1, 2, \ldots, m$, with vehicle 1 serving as the leader. Every following vehicle, denoted as $i > 1$, comes equipped with sensors that measure the distance to the vehicle directly ahead. The inter–vehicle distance is defined as $(d_i(t) := x_{i-1}(t) - x_i(t) - d_0)$ for $(i = 2, 3, \ldots, m)$. Since $\dot{x}_{i-1}(t) = v_{i-1}(t)$, and $\dot{x}_i(t) = v_i(t)$ differentiating the inter–vehicle distance yields $\dot{d}_i(t) = \dot{x}_{i-1}(t) - \dot{x}_i(t) = v_{i-1}(t) - v_i(t)$, $i = 2, 3, \ldots, m$. Thus, the distance dynamics depend on the relative velocity between two consecutive vehicles and do not assume that the preceding vehicle is stationary. Here, $x_i(t)$ represents the position of vehicle i at time t, while d_0 stands for a minimum safe gap, which accounts for both the length of the vehicle and an additional required clearance between two successive vehicles, as illustrated in Fig. 1. The lead vehicle, $i = 1$, is assumed to maintain a constant reference velocity v_0 using a properly designed velocity controller. The entire platoon vehicle is expected to meet the following criteria as outlined in reference [31].

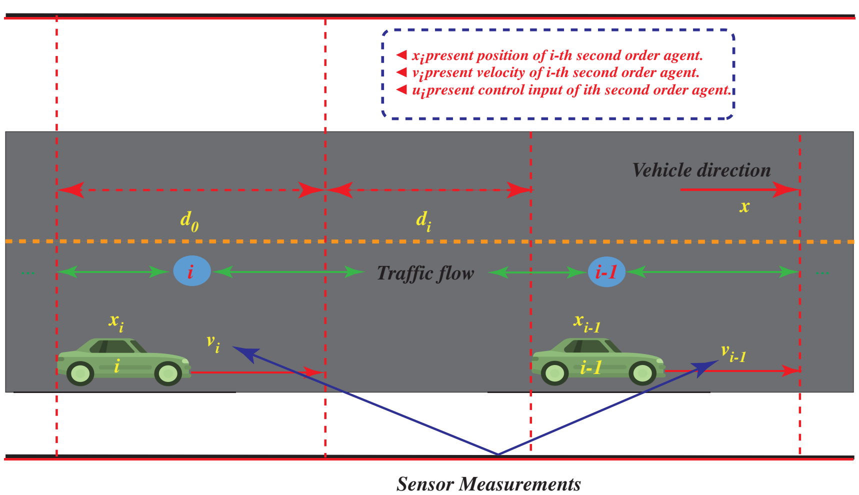

Figure 1: Two vehicles in a platoon configuration.

There are some basic necessary conditions. Every vehicle in the platoon should move at the same speed as the leader. That is, $\lim_{t\to\infty} \left| v_i(t) - v_1(t) \right| = 0$, $i = 2, 3, \ldots, m$, where $v_i(t)$ stands for the speed of vehicle i. The gap between two vehicles ought to grow as their speed increases. More precisely, the distance each follower keeps from the car ahead should eventually match a value proportional to its own speed, for example $\lim_{t\to\infty}\left|d_i(t)-\kappa v_i(t)\right| = 0$, $i = 2,3,\ldots,m$. Here, κ is what we call the time–headway coefficient. This coefficient determines the following distance as a function of speed. No vehicle should ever move in reverse, meaning $v_i(t) \geq 0$, $t \geq 0$, $i = 1,2,\ldots,m$. Thus, every vehicle moves forward or remains stationary. Finally, the distance $d_i(t) > 0$ factor should be greater than zero for all $i = 2,\ldots,m$.

Each follower vehicle asymptotically synchronizes its velocity with the preceding vehicle while maintaining the desired inter-vehicle spacing. The lead vehicle and a few following vehicles that have both position and velocity sensors are modelled as second-order agents in this platoon setup (1), whilst other following vehicles that can only measure position are modelled as first-order agents (2). Real-world car fleets, where various cars have varying degrees of automation, are reflected in this heterogeneity. In order to meet the platoon criteria of speed matching and safe distance keeping outlined in Section 3, the control objective is to achieve both position consensus and velocity consensus (as indicated in Section 3) among all vehicles.

4 Heterogeneous Multi–Agent System for Platoon Model Based on Event–Triggered Mechanism

Consider a heterogeneous multi–agent system for a vehicle platoon, consisting of both first–order and second–order agents. Specifically, the first group of agents are second–order agents, and the remaining agents are first-order agents. The dynamic model of the second-order multi-agent system is given by:

$$\begin{cases}\dot{x}_i(t) = v_i(t)\\ \dot{v}_i(t) = u_i(t), \quad i = 1,2,3,\ldots,m\end{cases} \tag{1}$$

In the above equation, $x_i(t) \in \mathcal{R}^x$, $v_i(t) \in \mathcal{R}^v$, and $u_i(t) \in \mathcal{R}^u$ represent the position, velocity, and control input of the ith second–order agent, respectively. The dynamic model of the first–order multi–agent system is:

$$\dot{x}_i(t) = u_i(t), \quad i = (m+1),(m+2),\ldots,n \tag{2}$$

Let m be the number of second-order agents and n the total number of agents ($n > m$). In the above equation, $x_i(t) \in \mathcal{R}^x$, and $u_i(t) \in \mathcal{R}^u$, represent the position and control input of the ith first–order agent, respectively. The structure of the agent node is shown in Fig. 2.

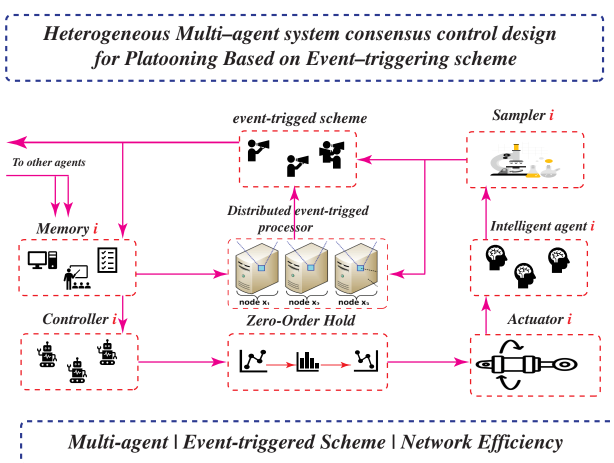

Figure 2: Structure of the ith intelligent agent node.

Definition 1: *The closed–loop heterogeneous multi–agent systems (1) and (2) are said to achieve asymptotic consensus if its trajectories satisfy the following limits:*

$$\begin{cases} \lim_{t\to\infty} \left\| v_i(t) - v_{i-1}(t) \right\| = 0, & i, j \in \mathcal{I}_n = \{2, \ldots, m\} \\ \lim_{t\to\infty} \left\| d_i(t) - \kappa v_i(t) \right\| = 0, & i, j \in \mathcal{I}_m = \{2, \ldots, m\} \end{cases} \tag{3}$$

Remark 1: *Eq. (3) defines the desired consensus objective of the heterogeneous multi-agent system. Under the proposed distributed control protocol and event-triggering mechanism, and provided that the LMI conditions derived in Section 5 are satisfied, the closed-loop system asymptotically achieves the consensus behavior specified in Eq. (3). In terms of platooning, this ensures that inter-vehicle distances stabilise to a constant value (the required time-headway $\kappa v_i(t)$), and string stability is attained because the lead vehicle's disturbances do not intensify throughout the chain.*

Assumption 1: *The communication topology graph $\mathcal{G}$ of the multi–agent system is an undirected connected graph.*

Assumption 2: *Both the actuator and the controller operate in an event-driven manner, while the sensor operates in a time–driven manner, with sampling period of $\hbar$, with $\hbar > 0$, respectively.*

Firstly, the following consensus protocols are designed for heterogeneous multi–agent systems (1) and (2):

$$\begin{aligned} u_i(t) &= -\mathcal{K}_1\left\{ \sum_{j\in\mathcal{N}_i^1} a_{ij}\Big((x_i(k\hbar) - x_j(k\hbar) \Big) \right\} - \mathcal{K}_1\left\{ \sum_{j\in\mathcal{N}_i^2} a_{ij}\Big((v_i(k\hbar) - v_j(k\hbar) \Big) \right\}, \ i \in \mathcal{I}_m \\ u_i(t) &= -\mathcal{K}_2\left\{ \sum_{j\in\mathcal{N}_i} a_{ij}\Big((x_i(k\hbar) - x_j(k\hbar) \Big) \right\}, i = (m+1), (m+2), \ldots, \mathcal{N} \end{aligned} \tag{4}$$

Remark 2: *$\mathcal{N}_i^1$ and $\mathcal{N}_i^2$ denote the neighbor sets of the ith second–order and first–order agents, respectively. It is clear that $\mathcal{N}_i = \mathcal{N}_i^1 \cup \mathcal{N}_i^2$, $\mathcal{K}_1$ and $\mathcal{K}_2$ are the gain matrices of the consensus controllers to be designed.*

Given the limited network communication resources, this research adopts an event–triggered mechanism to reduce the number of transmissions of the state information of agent i, thereby lowering the update frequency of controller i and the amount of information transmitted over the network to neighboring agents. Let $t_s^i\hbar$ denote the ith transmission instant of the position information of agent i, and let $t_\ell^i\hbar$ denote the ith ($\ell = 0, 1, 2, \ldots, i \in \mathcal{I}_m; j \in \mathcal{N}_i^1$) transmission instant of the velocity information of agent i. Thus, the transmission states of the position and velocity information of agent i can be described as follows:

$$\begin{aligned} \hat{x}_i(k\hbar) &= x_i(t_s^i\hbar), \quad k \in \left[t_s^i, t_{s+1}^i \right), \ i \in \mathcal{I}_n \\ \hat{v}_i(k\hbar) &= v_i(t_\ell^i\hbar), \quad k \in \left[t_\ell^i, t_{\ell+1}^i \right), \ i \in \mathcal{I}_m \end{aligned} \tag{5}$$

The next position information transmission time is defined as:

$$t_{s+1}^i\hbar = \inf\left\{ t : t > (\xi_1 t_s^i + \hbar), \ g_i(t) > 0 \right\} \tag{6}$$

The next speed information transmission moment is defined as:

$$t_{\ell+1}^i\hbar = \inf\left\{ t : t > (\xi_2 t_\ell^i + \hbar), \ f_i(t) > 0 \right\} \tag{7}$$

Remark 3: *From Eqs. (6) and (7) that an information transmission interval is always longer than one sampling period. Even when the system satisfies the triggering condition in every sampling period during a certain information transmission phase, the transmission interval can still be made longer than one sampling period by adjusting the parameters ξ_1, and ξ_2 as appropriate, thereby reducing bandwidth occupancy throughout the entire information transmission process.*

Where $(\xi_1, \xi_2) \geq 1$ are tuning parameters and $g_i(t)$ and $f_i(t)$ are event–triggering functions. The proposed event-triggering mechanism is designed as follows:

$$\begin{aligned}
&For\ second\text{–}order\ agents\ (position): g_i(t) = e_{xi}^T(k\hbar)\rho_1 e_{xi}(k\hbar) - \sigma_1 \mu_{xi}^T(k\hbar)\rho_1\mu_{xi}(k\hbar) > 0,\ i = 1, 2, \ldots, m \\
&For\ second\text{–}order\ agents\ (velocity):\ f_i(t) = e_{vi}^T(k\hbar)\rho_2 e_{vi}(k\hbar) - \sigma_2 \mu_{vi}^T(k\hbar)\rho_2\mu_{vi}(k\hbar) > 0,\ i = 1, 2, \ldots, m \\
&For\ First\text{–}order\ agents: \qquad g_i(t) = e_{xi}^T(k\hbar)\rho_3 e_{xi}(k\hbar) - \sigma_3 \mu_{xi}^T(k\hbar)\rho_3\mu_{xi}(k\hbar) > 0,\ i = (m+1), \ldots, n
\end{aligned} \tag{8}$$

where

$$\begin{aligned}
e_{xi}(k\hbar) &= x_i(k\hbar) - \hat{x}_i(k\hbar), \quad i \in \mathcal{I}_n, \quad k \in \left[t_s^i, t_{s+1}^i\right) \\
e_{vi}(k\hbar) &= v_i(k\hbar) - \hat{v}_i(k\hbar), \quad i \in \mathcal{I}_m, \quad k \in \left[t_\ell^i, t_{\ell+1}^i\right)
\end{aligned} \tag{9}$$

The parameters $\sigma_1, \sigma_2, \sigma_3$ are positive, dimensionless trigger-threshold coefficients. The parameter σ_1 is associated with the position transmission of the second-order agents, σ_2 is associated with their velocity transmission, and σ_3 is associated with the position transmission of the first-order agents. A transmission is generated when the weighted local update error exceeds the corresponding weighted neighbor-disagreement threshold $e_i^T \rho_k e_i > \sigma_k \mu_i^T \rho_k \mu_i$. Therefore, σ_k regulates the communication–performance trade-off of the corresponding triggering channel. Furthermore, we define:

$$\begin{aligned}
\mu_{xi}(k\hbar) &= \sum\nolimits_{j \in \mathcal{N}_i} a_{ij}\left[x_i(k\hbar) - x_j(k\hbar)\right] \\
\mu_{vi}(k\hbar) &= \sum\nolimits_{j \in \mathcal{N}_i^1} a_{ij}\left[v_i(k\hbar) - v_j(k\hbar)\right]
\end{aligned} \tag{10}$$

These equations include the agent node, its neighboring agent nodes, and the controller input information for node i at the most recent sampling instant. The scalars σ_1, σ_2, $\sigma_3 > 0$ are the threshold coefficients associated with the second-order position trigger, the second-order velocity trigger, and the first-order position trigger, respectively. They scale the corresponding neighbor-disagreement terms and regulate the communication–performance trade–off. The matrices $\rho_k = \rho_k^T > 0$, $k = 1, 2, 3$, are symmetric positive–definite weighting matrices of appropriate dimensions. They define the quadratic metrics used to evaluate the local information-update errors and neighbor-disagreement signals and are determined from the derived LMI conditions. The scalar thresholds σ_k and weighting matrices ρ_k are distinct design quantities; σ_k does not modify or adjust ρ_k.

Remark 4: *Compared with existing literature, the proposed triggering mechanism depends not only on the information update of the agent itself but also to the information of neighboring agents. Here, $\mu_{xi}(k\hbar)$, and $\mu_{vi}(k\hbar)$ describe the position and velocity information update status of the entire multi–agent system. When the whole system approaches toward consensus, i.e., $\lim_{k\to\infty} \mu_{xi}(k\hbar) = 0$, and $\lim_{k\to\infty} \mu_{vi}(k\hbar) = 0$. The information will be transmitted only when Eqs. (6) and (7) satisfied. This allows the system to be better maintained after it has reached consensus.*

Remark 5: *The parameters ξ_1 and ξ_2 determine the minimum transmission intervals and satisfy $\xi_1, \xi_2 \geq 1$. In contrast, σ_k, $k = 1, 2, 3$, are the threshold parameters of the event-triggering functions. As $\sigma_k \to 0^+$, the corresponding triggering condition approaches $e_i^T(k\hbar)\rho_k e_i(k\hbar) > 0$. Consequently, any nonzero local update error can activate the associated trigger after the minimum transmission interval imposed by Eqs. (6) and (7) has elapsed. Conversely, increasing σ_k raises the relative threshold associated with the neighbor-disagreement term and generally reduces the triggering frequency. Therefore, ξ_1, ξ_2 and $\sigma_1, \sigma_2, \sigma_3$ provide separate tuning of the minimum transmission interval and trigger sensitivity, respectively.*

Based on the above event–triggering scenario, the following consensus control protocol can be designed as follows:

$$
\begin{aligned}
u_i(t) &= -\mathcal{K}_1\left\{\sum\nolimits_{j\in\mathcal{N}_i^1} a_{ij}\left((\hat{x}_i(k\hbar) - \hat{x}_j(k\hbar))\right)\right\} - \mathcal{K}_1\left\{\sum\nolimits_{j\in\mathcal{N}_i^2} a_{ij}\left((\hat{v}_i(k\hbar) - \hat{v}_j(k\hbar))\right)\right\},\ i \in \mathcal{I}_m \\
u_i(t) &= -\mathcal{K}_2\left\{\sum\nolimits_{j\in\mathcal{N}_i} a_{ij}\left((\hat{x}_i(k\hbar) - \hat{x}_j(k\hbar))\right)\right\}, i = (m+1), (m+2), \ldots, \mathcal{N}
\end{aligned} \tag{11}
$$

It is obtained from the Eqs. (10) and (11).

$$
\begin{aligned}
u_i(t) = -\mathcal{K}_1 \sum\nolimits_{j\in\mathcal{N}_i} a_{ij}\left[x_i(k\hbar) - x_j(k\hbar) - e_{xi}(k\hbar) + e_{xj}(k\hbar)\right] - \mathcal{K}_1 \sum\nolimits_{j\in\mathcal{N}_i^2} a_{ij}\Big[v_i(k\hbar) \\
- v_j(k\hbar) \underbrace{-e_{vi}(k\hbar) + e_{vj}(k\hbar)}_{}\Big],\ i \in \mathcal{I}_m
\end{aligned} \tag{12}
$$

$$
\begin{aligned}
u_i(t) = -\mathcal{K}_2 \sum\nolimits_{j\in\mathcal{N}_i} a_{ij}\left[x_i(k\hbar) - x_j(k\hbar) - e_{xi}(k\hbar) + e_{xj}(k\hbar)\right], i = (m+1), (m+2), \ldots, \mathcal{N}, \\
t \in \left[k\hbar, (k+1)\hbar\right)
\end{aligned} \tag{12}
$$

Then Eqs. (1) and (2) can be converted to:

$$
\begin{aligned}
\dot{x}_i(t) &= v_i(t) \\
\dot{v}_i(t) &= -\mathcal{K}_1 \sum_{j\in\mathcal{N}_i} a_{ij}\left[x_i(k\hbar) - x_j(k\hbar) - e_{xi}(k\hbar) + e_{xj}(k\hbar)\right] - \mathcal{K}_1 \sum_{j\in\mathcal{N}_i^2} a_{ij}\Big[v_i(k\hbar) - v_j(k\hbar) \\
&\quad - e_{vi}(k\hbar) + e_{vj}(k\hbar)\Big], \quad i \in \mathcal{I}_m \\
\dot{x}_i(t) &= -\mathcal{K}_2 \sum_{j\in\mathcal{N}_i} a_{ij}\left[x_i(k\hbar) - x_j(k\hbar) - e_{xi}(k\hbar) + e_{xj}(k\hbar)\right], i = (m+1), (m+2), \ldots, \mathcal{N}, \\
&\quad t \in \left[k\hbar, (k+1)\hbar\right)
\end{aligned} \tag{13}
$$

Next, we define the augmented matrices as follows:

$$
\begin{aligned}
x^T(k\hbar) &= \begin{bmatrix} x_1^T(k\hbar) & x_2^T(k\hbar) & \ldots & x_m^T(k\hbar) \end{bmatrix}^T \in \mathcal{R}^{m\times 1} \\
v^T(k\hbar) &= \begin{bmatrix} v_1^T(k\hbar) & v_2^T(k\hbar) & \ldots & v_m^T(k\hbar) \end{bmatrix}^T \in \mathcal{R}^{m\times 1} \\
e_{xi}^T(k\hbar) &= \begin{bmatrix} e_{x1}^T(k\hbar) & e_{x2}^T(k\hbar) & \ldots & e_{xm}^T(k\hbar) \end{bmatrix}^T; i \in \mathcal{I}_m \\
e_{vi}^T(k\hbar) &= \begin{bmatrix} e_{v1}^T(k\hbar) & e_{v2}^T(k\hbar) & \ldots & e_{vm}^T(k\hbar) \end{bmatrix}^T; i \in \mathcal{I}_m \\
\mathcal{Z}(k\hbar) &= \begin{bmatrix} x^T(k\hbar) & v^T(k\hbar) & \mathcal{X}^T(k\hbar) \end{bmatrix}^T \in \mathcal{R}^{(m+n)\times 1} \\
\mathcal{W}(k\hbar) &= \begin{bmatrix} e_x^T(k\hbar) & e_v^T(k\hbar) & \mathcal{E}^T(k\hbar) \end{bmatrix}^T \in \mathcal{R}^{(m+n)\times 1}
\end{aligned}
$$

$$\mathcal{X}(k\hbar) = \begin{bmatrix} x_{m+1}^T(k\hbar) & x_{m+2}^T(k\hbar) & \dots & x_n^T(k\hbar) \end{bmatrix}^T \in \mathcal{R}^{(n-m)\times p}$$
$$\mathcal{E}(k\hbar) = \begin{bmatrix} e_{m+1}^T(k\hbar) & e_{m+2}^T(k\hbar) & \dots & e_n^T(k\hbar) \end{bmatrix}^T \in \mathcal{R}^{(n-m)\times p}$$

Now, we present the Laplacian matrix $\mathcal{L} \in \mathcal{R}^{n\times n}$, where $\mathcal{L}_{11} \in \mathcal{R}^{(n-m)\times(n-m)}$, $\mathcal{L}_{12} \in \mathcal{R}^{(n-m)\times m}$, $\mathcal{L}_{21} \in \mathcal{R}^{m\times(n-m)}$, $\mathcal{L}_{22} \in \mathcal{R}^{m\times m}$.

$$\mathcal{L} = \begin{bmatrix} \mathcal{L}_{11} & \mathcal{L}_{12} \\ \mathcal{L}_{21} & \mathcal{L}_{22} \end{bmatrix}$$

Substituting (11) into (1) and (2) and using the definitions in (14), we obtain the compact form (14) after collecting terms involving $\mathcal{Z}(k\hbar)$ and $\mathcal{W}(k\hbar)$. From the Eq. (13), it can be obtained:

$$\dot{\chi}(t) = \mathcal{Z}_{11}\mathcal{X}(k\hbar) + \mathcal{W}_{11}\mathcal{W}(k\hbar), \quad k \in \left[t_\ell^i, t_{\ell+1}^i\right) \tag{14}$$

For notational convenience in the subsequent stability analysis, define $\chi(t) := \mathcal{Z}(t)$, $\chi(k\hbar) := \mathcal{Z}(k\hbar)$. Thus, $\chi(t)$ is not a transformed state; it is the same augmented state vector previously denoted by $\mathcal{Z}(t)$, where

$$\mathcal{Z}_{11} = \begin{bmatrix} 0 & \mathcal{I}_{m\times m} & 0 \\ k_1\mathcal{L}_{22} & k_1\mathcal{L}_{22} & k_1\mathcal{L}_{21} \\ k_2\mathcal{L}_{12} & 0 & k_2\mathcal{L}_{11} \end{bmatrix}$$
$$\mathcal{W}_{11} = \begin{bmatrix} 0 & 0 & 0 \\ k_1\mathcal{L}_{22} & k_1\mathcal{L}_{22} & k_1\mathcal{L}_{21} \\ k_2\mathcal{L}_{12} & 0 & k_2\mathcal{L}_{11} \end{bmatrix}$$

To facilitate analysis, let $d(t) = t - k\hbar$, where $k\hbar \le t \le (k+1)\hbar$ and $k \in \mathcal{N}$. It is clear that $t \ne k\hbar$, $\dot{d}(t) = 1$. When $t = k\hbar$, we have $0 \le d(t) \le \hbar$. Therefore, Eq. (14) can be transformed as follows:

$$\dot{\chi}(t) = \mathcal{Z}_{11}\chi(k\hbar) + \mathcal{W}_{11}\mathcal{W}(k\hbar),\ t \in \left[k\hbar, (k+1)\hbar\right) \tag{15}$$

Then with the definition of $d(t) = t - k\hbar$, our closed–loop (16) model becomes:

$$\dot{\chi}(t) = \mathcal{Z}_{11}\chi(t - d(t)) + \mathcal{W}_{11}\mathcal{W}(t - d(t)),\ t \in \left[k\hbar, (k+1)\hbar\right) \tag{16}$$

Thus, the systems (1) and (2) achieve asymptotic consensus when and only if the closed–loop system (16) is asymptotically stable. For ease of analysis, we define $\mathcal{E}_1 = \begin{bmatrix} I_{m\times m} & 0 & 0 \end{bmatrix}$, $\mathcal{E}_2 = \begin{bmatrix} 0 & I_{m\times m} & 0 \end{bmatrix}$, $\mathcal{E}_3 = \begin{bmatrix} 0 & 0 & I_{m\times m} \end{bmatrix}$, and $\mathcal{E}_{13} = \begin{bmatrix} I_{m\times m} & 0 & 0 \\ 0 & 0 & I_{m\times m} \end{bmatrix}$, $e_x(k\hbar) = \mathcal{E}_1\mathcal{W}(k\hbar)$, $e_v(k\hbar) = \mathcal{E}_2\mathcal{W}(k\hbar)$, $\mathcal{E}_x(k\hbar) = \mathcal{E}_3\mathcal{W}(k\hbar)$. For subsequent proof, when the trigger conditions are not satisfied, then the Eq. (8) can be converted to:

$$\mathcal{W}^T(k\hbar)\mathcal{E}_1^T\rho_1\big(\mathcal{E}_1\mathcal{W}(k\hbar)\big) < \sigma_1\left\{\left[\left[\begin{array}{cc}\mathcal{L}_{22} & \mathcal{L}_{21}\end{array}\right]\otimes\mathcal{I}_p\big(\mathcal{E}_{13}\mathcal{Z}(k\hbar)\big)\right]^T\right\}\rho_1$$
$$\times\left[\begin{array}{cc}\mathcal{L}_{22} & \mathcal{L}_{21}\end{array}\right]\otimes\mathcal{I}_p\big(\mathcal{E}_{13}\mathcal{Z}(k\hbar)\big)$$
$$\mathcal{W}^T(k\hbar)\mathcal{E}_2^T\rho_2\big(\mathcal{E}_2\mathcal{W}(k\hbar)\big) < \sigma_2\left\{\left[\mathcal{L}_{22}\otimes\mathcal{I}_p\big(\mathcal{E}_2\mathcal{Z}(k\hbar)\big)\right]^T\right\}\rho_2$$
$$\times\left[\mathcal{L}_{22}\otimes\mathcal{I}_p\big(\mathcal{E}_2\mathcal{Z}(k\hbar)\big)\right] \tag{17}$$
$$\mathcal{W}^T(k\hbar)\mathcal{E}_3^T\rho_3\big(\mathcal{E}_3\mathcal{W}(k\hbar)\big) < \sigma_3\left\{\left[\mathcal{L}_{12}\quad\mathcal{L}_{11}\right]\otimes\mathcal{I}_p\big(\mathcal{E}_{13}\mathcal{Z}(k\hbar)\big)\right]^T\right\}\rho_3$$
$$\times\left[\mathcal{L}_{12}\quad\mathcal{L}_{11}\right]\otimes\mathcal{I}_p\big(\mathcal{E}_{11}\mathcal{Z}(k\hbar)\big) \tag{18}$$

Before proceeding to the main stability section, the authors will present some Lemmas, which help in the formation of LMIs.

Lemma 1 ([32]): *For any constant matrices $\mathcal{R}\in\mathcal{R}^{n\times n}$, $\mathcal{R}=\mathcal{R}^T>0$, $\mathcal{H}\in R^{n\times k}$, and a time–varying function $0<d(t)\leq\hbar$ satisfying $\dot{\delta}:\left[-\hbar,0\right]\to\mathcal{R}^n$, let the vector function $\dot{\delta}$ be such that $\int_{t-d(t)}^{t}\dot{\delta}(s)=\mathcal{F}\varphi(t)d(s)$, where $\varphi(t)\in\mathcal{R}^k$. Then the following inequality holds:*

$$-\int_{t-d(t)}^{t}\dot{\delta}(t)\mathcal{R}\dot{\delta}(s)\leq-\varphi^T(t)\Big(d(t)\mathcal{H}^T\mathcal{R}^{-1}\mathcal{H}-\mathcal{F}^T\mathcal{H}-\mathcal{H}^T\mathcal{F}\Big)\varphi(t) \tag{19}$$

Lemma 2 ([32]): *Assume there exist real numbers $\xi_{\bar{k}}>0\,(\bar{k}=1,2,3.)$ and a Lyapunov function $\mathcal{V}\Big(t,\chi(t),\dot{\chi}(t)\Big)$. For the corresponding solution of the system (16) $\chi(t)$ for $t\geq t_0$, the function $\mathcal{V}\Big(t,\chi(t),\dot{\chi}(t)\Big)$ is continuously differentiable when $t\neq k\hbar$ and satisfies the following conditions:*

$$\xi_1\Big\|\chi(t)\Big\|^2\leq\mathcal{V}\Big(t,\chi(t),\dot{\chi}(t)\Big)\leq\xi_2\Big\|\chi(t)\Big\|^2 \tag{20}$$

$$\mathcal{V}\Big(t,\chi(t),\dot{\chi}(t)\Big)\leq-\xi_3\Big\|\chi(t)\Big\|^2,\ t\neq k\hbar \tag{21}$$

$$\lim_{t\to k\hbar^-}\mathcal{V}\Big(t,\chi(t),\dot{\chi}(t)\Big)\geq\mathcal{V}\Big(t,\chi(t),\dot{\chi}(t)\Big)\Big|_{t=k\hbar} \tag{22}$$

Lemma 3 ([33]): *Let $\mathcal{X}$, and $\mathcal{Y}$ with appropriate dimensions. If there exists a constant $\nu>0$, then the following holds:*

$$\mathcal{X}^T\mathcal{Y}+\mathcal{Y}^T\mathcal{X}\leq\nu\mathcal{X}^T\mathcal{X}+\frac{1}{\nu}\mathcal{Y}^T\mathcal{Y} \tag{23}$$

5 Co–Design of Distributed Event-Triggering Mechanism For Consensus Control

In this section, delay-dependent sufficient conditions are derived for the co-design of the distributed event-triggering mechanism and consensus controller for the heterogeneous multi-agent system represented by the closed-loop model in Eq. (16). The asymptotic stability of the event-triggered closed-loop system, established under the derived LMI conditions, guarantees convergence to the prescribed platoon-consensus objective. In particular, the vehicle velocities synchronize with the leader's reference velocity, and the spacing errors converge to zero according to the adopted time-headway policy. We first present the following corollary, which provides general requirements for the resultant model (16), is first presented.

The authors note that the following co-design technique is novel for heterogeneous MASs before presenting the LMI conditions: the controller gains $(\mathcal{K}_1, \mathcal{K}_2)$ and the event-triggering thresholds (ρ_1, ρ_2, ρ_3) are derived from a single set of LMIs (33) and (34). The majority of current literature [19,24] construct the controller before the event trigger, which is not ideal.

Corollary 1: *Given $\hbar > 0$, under the new event–triggered mechanisms (8), there exist real numbersk_1, and k_2; appropriately dimensional real matrices $\mathcal{P} > 0$, $\mathcal{X} > 0$, $\mathcal{R} > 0$, $\Psi > 0$, $Y > 0$, $\rho_{\bar{k}} > 0$, ($\bar{k} = 1, 2, 3$.) and matrices $\mathcal{M}_l > 0$, ($l = 1, 2$.) such that the following matrix inequalities hold:*

$$\begin{bmatrix} \Lambda_{11} + \hbar\aleph_{11} & \hbar\mathcal{F}^T(Y+\mathcal{R}) & \hbar\mathcal{M}_1^T \\ (\bullet) & -\hbar(Y+\mathcal{R}) & 0 \\ (\bullet) & (\bullet) & -\hbar\mathcal{R} \end{bmatrix} < 0 \tag{24}$$

$$\begin{bmatrix} \Lambda_{11} & \hbar\mathcal{F}^T\mathcal{R} & \hbar\mathcal{M}_2^T \\ (\bullet) & -\hbar\mathcal{R} & 0 \\ (\bullet) & (\bullet) & -\hbar(Y+\mathcal{R}) \end{bmatrix} < 0 \tag{25}$$

Then the closed–loop system (2) is globally asymptotically stable. Define:

$$\begin{aligned}
\Lambda_{11} = {} & \nu_1^T\mathcal{P}^T\mathcal{F} + \mathcal{F}^T\mathcal{P}\nu_1 + \nu_1^T\Psi\nu_1 - \nu_3^T\Psi\nu_3 - \nu_{12}^T\mathcal{X}\nu_{12} \\
& - \nu_{23}^T\mathcal{M}_1 - \mathcal{M}_1^T\nu_{23} - \nu_{12}^T\mathcal{M}_2 - \mathcal{M}_2^T\nu_{12} - \nu_4^T\left(\mathcal{E}_1^T\rho_1\mathcal{E}_1\right)\nu_4 \\
& - \nu_4^T\left(\mathcal{E}_2^T\rho_2\mathcal{E}_2\right)\nu_4 - \nu_4^T\left(\mathcal{E}_3^T\Phi_3\mathcal{E}_3\right)\nu_4 + \varphi^T(t)\nu_2^T \\
& \left\{\sigma_1\{[\mathcal{L}_{22} \quad \mathcal{L}_{21}] \otimes \mathcal{I}_p\mathcal{E}_{13}\}^T\rho_1[\mathcal{L}_{22} \quad \mathcal{L}_{21}] \otimes \mathcal{I}_p\mathcal{E}_{13}\right. \\
& + \left\{\nu_2[\mathcal{L}_{22} \otimes \mathcal{I}_p\mathcal{E}_2]^T\rho_2[\mathcal{L}_{22} \otimes \mathcal{I}_p\mathcal{E}_2]\right\} + \left\{\nu_3\{[\mathcal{L}_{12} \quad \mathcal{L}_{13}]\right. \\
& \left.\left.\otimes \mathcal{I}_p\mathcal{E}_{13}\}^T\rho_3[\mathcal{L}_{12} \quad \mathcal{L}_{13}] \otimes \mathcal{I}_p\mathcal{E}_{13}\right\}\right\}\nu_2\varphi(t)
\end{aligned}$$

$$\aleph_{11} = \nu_{12}^T\mathcal{X}\mathcal{F} + \mathcal{F}^T\mathcal{X}\nu_{12}, \ \mathcal{F} = \mathcal{A}\nu_2 + \mathcal{B}\nu_4,$$

$$\nu_1 = \begin{bmatrix} I & 0 & 0 \end{bmatrix}, \ \nu_2 = \begin{bmatrix} 0 & I & 0 \end{bmatrix}, \ \nu_3 = \begin{bmatrix} 0 & 0 & I \end{bmatrix}, \ \nu_4 = \begin{bmatrix} 0 & 0 & 0 & I \end{bmatrix}$$

Proof: The Lyapunov-Krasovskii functional for the closed-loop system is chosen as follows:

$$\mathcal{V}\left(t, \chi(t), \dot{\chi}(t)\right) = \mathcal{V}_1\left(t, \chi(t), \dot{\chi}(t)\right) + \mathcal{V}_2\left(t, \chi(t), \dot{\chi}(t)\right), \ t \in \left[k\hbar, (k+1)\hbar\right) \tag{26}$$

where

$$\mathcal{V}_1\left(t, \chi(t), \dot{\chi}(t)\right) = \chi(t)^T\mathcal{P}\chi(t) + \int_{t-\hbar}^{t}\chi(\alpha)^T\Psi\chi(\alpha)d\alpha + \int_{-\hbar}^{0}\int_{t+\beta}^{t}\dot{\chi}(\alpha)^T\mathcal{R}\dot{\chi}(\alpha)d\alpha d\beta$$

$$\begin{aligned}
\mathcal{V}_2\left(t, \chi(t), \dot{\chi}(t)\right) = {} & \left(\hbar - d(t)\right)\left\{\left[\chi(t) - \chi(t-d(t))\right]^T\mathcal{X}\left[\chi(t) - \chi(t-d(t))\right]\right. \\
& \left. + \int_{t-d(t)}^{t}\dot{\chi}(\alpha)^TY\dot{\chi}(\alpha)d\alpha\right\}, \ \beta \in \left[-\hbar, 0\right]
\end{aligned}$$

According to the Lemma 2, the term $\mathcal{V}_1\Big(t, \chi(t), \dot{\chi}(t)\Big) \geq 0$, and $\mathcal{V}_2\Big(t, \chi(t), \dot{\chi}(t)\Big) > 0$. Thus $t = k\hbar$, then second condition in the Lemma 2 is established. Take the time derivative of (26), where $t \in \Big[k\hbar, (k+1)\hbar\Big)$, with $\dot{\hbar}(t) = 1$, and $t \neq k\hbar$.

$$\begin{aligned}
\dot{\mathcal{V}}\Big(t, \chi(t), \dot{\chi}(t)\Big) = {} & 2\chi(t)^T\mathcal{P}\dot{\chi}(t) + \chi(t)^T\Psi\chi(t) - \chi(t-\hbar)^T\Psi\chi(t-\hbar) + \hbar\dot{\chi}(t)^T\mathcal{R}\dot{\chi}(t) \\
& - \int_{t-\hbar}^{t} \dot{\chi}(\alpha)^T\mathcal{R}\dot{\chi}(\alpha)d\alpha - \Big[\chi(t) - \chi(t-d(t))\Big]^T\mathcal{X}\Big[\chi(t) - \chi(t-d(t))\Big] \\
& + \Big(\hbar - d(t)\Big)\Big\{\Big[\dot{\chi}(t) - \dot{\chi}(t-d(t))\Big]^T\mathcal{X}\Big[\chi(t) - \chi(t-d(t))\Big]\Big\} \\
& + \Big[\chi(t) - \chi(t-d(t))\Big]^T\mathcal{X}\Big[\dot{\chi}(t) - \dot{\chi}(t-d(t))\Big] \\
& + \Big(\hbar - d(t)\Big)\Big\{\Big[\dot{\chi}(\alpha)^TY\dot{\chi}(\alpha) - \dot{\chi}(t-d(t))^TY\dot{\chi}(t-d(t))\Big]\Big\} \\
& - \int_{t-d(t)}^{t} \dot{\chi}(\alpha)^TY\dot{\chi}(\alpha)d\alpha
\end{aligned} \tag{27}$$

Further computing with Lemma 1:

$$\begin{aligned}
& = \varphi^T(t)\Big[v_1^T\mathcal{P}\mathcal{F} + \mathcal{F}^T\mathcal{P}v_1 + v_1^T\Psi v_1 - v_3^T\Psi v_3 - v_{12}^T\mathcal{X}v_{12} - v_4^T\Big(\mathcal{E}_1^T\rho_1\mathcal{E}_1\Big)v_4 - v_4^T\Big(\mathcal{E}_2^T\rho_2\mathcal{E}_2\Big)v_4 \\
& - v_4^T\Big(\mathcal{E}_3^T\rho_3\mathcal{E}_3\Big)v_4 + (\hbar - d(t))\big(v_{12}^T\mathcal{X}\mathcal{F} + \mathcal{F}^T\mathcal{X}v_{12} + \mathcal{F}^T\mathcal{Y}\mathcal{F}\big)\Big]\varphi(t) + \psi_1 + \psi_2 + \mathcal{W}_4^T\Big(\mathcal{E}_1^T\rho_1\mathcal{E}_1\Big)\mathcal{W}_4 \\
& + +\mathcal{W}_4^T\Big(\mathcal{E}_2^T\rho_2\mathcal{E}_2\Big)\mathcal{W}_4 + \mathcal{W}_4^T\Big(\mathcal{E}_3^T\rho_3\mathcal{E}_3\Big)\mathcal{W}_4
\end{aligned}$$

So

$$\psi_1 = -\int_{t-\hbar}^{t} \dot{\chi}^T(\alpha)\mathcal{R}\dot{\chi}(\alpha)d\alpha, \quad \psi_2 = -\int_{t-d(t)}^{t} \dot{\chi}^T(\alpha)Y\dot{\chi}(\alpha)d\alpha,$$

With

$$\psi_1 + \psi_2 = -\int_{t-\hbar}^{t-d(t)} \dot{\chi}^T(\alpha)\mathcal{R}\dot{\chi}(\alpha)d\alpha - \int_{t-d(t)}^{t} \dot{\chi}^T(\alpha)(\mathcal{R} + Y)\dot{\chi}(\alpha)d\alpha$$

The terms $\int_{t-\hbar}^{t-d(t)} \dot{\chi}^T(\alpha)d\alpha = v_{23}\varphi(t)$, $\int_{t-d(t)}^{t} \dot{\chi}^T(\alpha)d\alpha = v_{12}\varphi(t)$ can be obtained from Lemma 3:

$$\begin{aligned}
\psi_1 + \psi_2 \leq \varphi^T(t)\Big\{ & (\hbar - d(t))\mathcal{M}_1^T\mathcal{R}^{-1}\mathcal{M}_1 - v_{23}^T\mathcal{M}_1 \\
& - \mathcal{M}_1^Tv_{23} + d(t)\mathcal{M}_2^T(\mathcal{R} + \mathcal{Y})^{-1}\mathcal{M}_2 - v_{12}^T\mathcal{M}_2 \\
& - \mathcal{M}_2^Tv_{12}\Big\}\varphi(t)
\end{aligned} \tag{28}$$

Add the left and right sides of the Formulas (17)–(19) to get the result:

$$\Rightarrow \mathcal{W}^T\left(\mathcal{E}_1^T\rho_1\mathcal{E}_1\right)\mathcal{W} + \mathcal{W}^T\left(\mathcal{E}_2^T\rho_2\mathcal{E}_2\right)\mathcal{W} + \mathcal{W}^T\left(\mathcal{E}_3^T\rho_3\mathcal{E}_3\right)\mathcal{W} < \mathcal{Z}^T(k\hbar)\mathcal{E}_{13}^T\left\{\sigma_1\{[\mathcal{L}_{22} \quad \mathcal{L}_{21}]\otimes\mathcal{I}_p\}^T \right.$$
$$\left.\rho_1[\mathcal{L}_{22} \quad \mathcal{L}_{21}]\otimes\mathcal{I}_p\right\}(\mathcal{E}_{13}\mathcal{Z}(k\hbar)) + (\mathcal{Z}^T(kh)\mathcal{E}_2^T)\left\{\sigma_2\{\mathcal{L}_{22}\otimes\mathcal{I}_p\}^T\rho_2[\mathcal{L}_{22}\otimes\mathcal{I}_p]\right\}(\mathcal{E}_2\mathcal{Z}(k\hbar))$$
$$+ \mathcal{Z}^T(k\hbar)\mathcal{E}_{13}^T\left\{\sigma_3\{[\mathcal{L}_{12} \quad \mathcal{L}_{13}]\otimes\mathcal{I}_p\}^T\rho_3[\mathcal{L}_{12} \quad \mathcal{L}_{13}]\otimes\mathcal{I}_p\right\}(\mathcal{E}_{13}\mathcal{Z}(k\hbar)) \tag{29}$$

So

$$\Rightarrow \mathcal{W}^T\left(\mathcal{E}_1^T\rho_1\mathcal{E}_1\right)\mathcal{W} + \mathcal{W}^T\left(\mathcal{E}_2^T\rho_2\mathcal{E}_2\right)\mathcal{W} + \mathcal{W}T\left(\mathcal{E}_3^T\rho_3\mathcal{E}_3\right)\mathcal{W}$$
$$< \varphi^T(t)\nu_2^T\mathcal{E}_{13}^T\left\{\sigma_1\{[\mathcal{L}_{22} \quad \mathcal{L}_{21}]\otimes\mathcal{I}_p\}^T\rho_1[\mathcal{L}_{22} \quad \mathcal{L}_{21}]\otimes\mathcal{I}_p\right\}$$
$$\left(\mathcal{E}_{13}\nu_2\varphi(t)\right) + \varphi^T(t)\nu_2^T\mathcal{E}_2^T\left\{\sigma_2\{\mathcal{L}_{22}\otimes\mathcal{I}_p\}^T\rho_2[\mathcal{L}_{22}\otimes\mathcal{I}_p]\right\}$$
$$\left(\mathcal{E}_2\nu_2\varphi(t)\right) + \varphi^T(t)\nu_2^T\mathcal{E}_{13}^T\left\{\sigma_3\{[\mathcal{L}_{12} \quad \mathcal{L}_{13}]\otimes\mathcal{I}_p\}^T\right.$$
$$\left.\rho_3[\mathcal{L}_{12} \quad \mathcal{L}_{13}]\otimes\mathcal{I}_p\right\}\left(\mathcal{E}_{13}\nu_2\varphi(t)\right) \tag{30}$$

Therefore, from the Eqs. (27), (28) and (30). It can be obtained:

$$\dot{\mathcal{V}}\left(t, \chi(t), \dot{\chi}(t)\right) \le \varphi^T(t)\Theta\varphi(t), \; t \in \left[k\hbar, (k+1)\hbar\right)$$

where

$$\Theta = \Lambda_{11} + \mho_1 + \left(\hbar - d(t)\right)\left(\aleph_{11} + \mho_2\right) + \hbar\mho_3$$
$$\mho_1 = \hbar\mathcal{F}^T\mathcal{R}\mathcal{F}, \; \aleph_{11} = \nu_{12}^T\mathcal{X}\mathcal{F} + \mathcal{F}\mathcal{X}\nu_{12}$$
$$\mho_2 = \mathcal{F}^T Y\mathcal{F} + \mathcal{M}_1^T\mathcal{R}^{-1}\mathcal{M}_1, \; \mho_3 = \mathcal{M}_2^T\left(\mathcal{R} + Y^{-1}\right)\mathcal{M}_2$$

Clearly, if $\Theta < 0$, then there exists $\xi_3 > 0$, such that $\mathcal{V}\left(t, \chi(t), \dot{\chi}(t)\right) \le -\xi_3\left\|\chi(t)\right\|^2$. From the Lemma 2, it follows that system (16) is asymptotically stable. Define $\lambda(t) = \frac{d(t)}{\hbar} \in [0, 1]$. Then, $\Theta(d(t))$ can be expressed as

$$\Theta(d(t)) = (1 - \lambda(t))\left[\Lambda_{11} + \mho_1 + \hbar\left(\aleph_{11} + \mho_2\right)\right] + \lambda(t)\left[\Lambda_{11} + \mho_1 + \hbar\mho_3\right].$$

Therefore, $\Theta(d(t))$ is a convex combination of its values at the two endpoints $d(t) = 0$ and $d(t) = \hbar$. Hence, $\Theta(d(t)) \prec 0$ for every $d(t) \in [0, \hbar]$ if both endpoint matrices are negative definite. Therefore, to ensure $\Theta < 0$, we can set:

$$\Lambda_{11} + \mho_1 + \hbar\left(\aleph_{11} + \mho_2\right) < 0 \tag{31}$$

$$\Lambda_{11} + \mho_1 + d(t)\mho_3 < 0 \tag{32}$$

According to the Schur complement, Eqs. (31) and (32) can be transformed into Eqs. (24) and (25), respectively. This completes the proof. □

Since inequalities (24) and (25) in Corollary 1 contain nonlinear terms, we propose the following corollary to convert them into solvable linear matrix inequalities.

Corollary 2: *Given $\hbar > 0$, under the new event–triggered mechanism (8), there exist real numbers k_1, k_2, $\mu_1 > 0$; and $\mu_2 > 0$ appropriately dimensional real matrices $\mathcal{P} > 0$, $\mathcal{X} > 0$, $\mathcal{R} > 0$, $\Psi > 0$, $Y > 0$, $\rho_{\bar{k}} > 0$, ($\bar{k} = 1, 2, 3.$) and matrices $\mathcal{M}_l > 0$, ($l = 1, 2.$) such that the following matrix inequalities hold:*

$$\begin{bmatrix} \tilde{\Lambda}_{11} & 0 & \hbar\mathcal{M}_1 & v_1^T\mathcal{P}^T + v_{12}^T\mathcal{X}^T & \mathcal{F}^T \\ (\bullet) & -\hbar(Y+\mathcal{R}) & 0 & \hbar(Y+\mathcal{R})^T & 0 \\ (\bullet) & (\bullet) & -\hbar\mathcal{R} & 0 & 0 \\ (\bullet) & (\bullet) & (\bullet) & -\mu_1\mathcal{I} & 0 \\ (\bullet) & (\bullet) & (\bullet) & (\bullet) & -\mu_1^{-1}\mathcal{I} \end{bmatrix} < 0 \tag{33}$$

$$\begin{bmatrix} \tilde{\Lambda}_{11} & 0 & \hbar\mathcal{M}_2^T & v_1^T\mathcal{P}^T & \mathcal{F}^T \\ (\bullet) & -\hbar\mathcal{R} & 0 & -\hbar\mathcal{R}^T & 0 \\ (\bullet) & (\bullet) & -\hbar(Y+\mathcal{R}) & 0 & 0 \\ (\bullet) & (\bullet) & (\bullet) & -\mu_2\mathcal{I} & 0 \\ (\bullet) & (\bullet) & (\bullet) & (\bullet) & -\mu_2^{-1}\mathcal{I} \end{bmatrix} < 0 \tag{34}$$

Therefore, the closed–loop system (16) is globally asymptotically stable. So,

$$\begin{aligned}\tilde{\Lambda}_{11} = {} & v_1^T\mathcal{P}^T\mathcal{F} + \mathcal{F}^T\mathcal{P}v_1 + v_1^T\Psi v_1 - v_3^T\Psi v_3 - v_{12}^T\mathcal{X}v_{12} \\ & - v_{23}^T\mathcal{M}_1 - \mathcal{M}_1^T v_{23} - v_{12}^T\mathcal{M}_2 - \mathcal{M}_2^T v_{12} - v_4^T\Big(\mathcal{E}_1^T\rho_1 \\ & \mathcal{E}_1\Big)v_4 - v_4^T\Big(\mathcal{E}_2^T\rho_2\mathcal{E}_2\Big)v_4 - v_4^T\Big(\mathcal{E}_3^T\rho_3\mathcal{E}_3\Big)v_4 + \varphi^T(t) \\ & v_2^T\Big\{\sigma_1\big\{[\mathcal{L}_{22} \quad \mathcal{L}_{21}]\otimes\mathcal{I}_p\mathcal{E}_{13}\big\}^T\rho_1[\mathcal{L}_{22} \quad \mathcal{L}_{21}]\otimes\mathcal{I}_p\mathcal{E}_{13} \\ & + \big\{v_2[\mathcal{L}_{22}\otimes\mathcal{I}_p\mathcal{E}_2]^T\rho_2[\mathcal{L}_{22}\otimes\mathcal{I}_p]\mathcal{E}_2\big\} + \big\{v_3\big\{[\mathcal{L}_{12} \quad \mathcal{L}_{11}] \\ & \otimes\mathcal{I}_p\mathcal{E}_{13}\big\}^T\rho_3[\mathcal{L}_{12} \quad \mathcal{L}_{11}]\otimes\mathcal{I}_p\mathcal{E}_{13}\big\}\Big\}v_2\varphi(t)\end{aligned}$$

Proof: From the Eq. (24), which can be written as:

$$\begin{bmatrix} \tilde{\Lambda}_{11} & 0 & \hbar\mathcal{M}_1^T \\ (\bullet) & -\hbar(Y+\mathcal{R}) & 0 \\ (\bullet) & (\bullet) & -\hbar\mathcal{R} \end{bmatrix} + \begin{bmatrix} \mathcal{F}^T \\ 0 \\ 0 \end{bmatrix}\begin{bmatrix} v_1^T\mathcal{P}^T + v_{12}^T\mathcal{X}^T \\ \hbar(Y+\mathcal{R})^T \\ 0 \end{bmatrix}^T + \begin{bmatrix} v_1^T\mathcal{P}^T + v_{12}^T\mathcal{X}^T \\ \hbar(Y+\mathcal{R})^T \\ 0 \end{bmatrix}\begin{bmatrix} \mathcal{F}^T \\ 0 \\ 0 \end{bmatrix}^T < 0 \tag{35}$$

From Lemma 3, Eq. (35) can be converted to Eq. (36):

$$\begin{bmatrix} \tilde{\Lambda}_{11} & 0 & \hbar\mathcal{M}_1^T \\ (\bullet) & -\hbar(Y+\mathcal{R}) & 0 \\ (\bullet) & (\bullet) & -\hbar\mathcal{R} \end{bmatrix} + \mu_1\begin{bmatrix} \mathcal{F}^T \\ 0 \\ 0 \end{bmatrix}\begin{bmatrix} \mathcal{F}^T \\ 0 \\ 0 \end{bmatrix}^T + \mu_1^{-1}\begin{bmatrix} v_1^T\mathcal{P}^T + v_{12}^T\mathcal{X}^T \\ \hbar(Y+\mathcal{R})^T \\ 0 \end{bmatrix}\begin{bmatrix} v_1^T\mathcal{P}^T + v_{12}^T\mathcal{X}^T \\ \hbar(Y+\mathcal{R})^T \\ 0 \end{bmatrix}^T < 0 \tag{36}$$

Then, by Schur complement, Eq. (36) can be transformed into Eq. (33), that is, Eq. (24) can be transformed into Eq. (33), and Eq. (25) can be transformed into Eq. (34). This completes the proof. □

Remark 6: *Current event-triggered consensus control techniques for multi-agent systems frequently have a number of serious drawbacks, especially when it comes to vehicle platooning. First off, a lot of traditional methods only concentrate on homogeneous multi-agent systems, in which every agent has the same dynamics. This leaves the more realistic problem of heterogeneous platoons—which include a combination of, say, first-order and second-order vehicles—largely unsolved. Second, these conventional approaches usually define the trigger conditions based only on the individual agent's state error (the difference between its current and last transferred state), ignoring the important information about the system's overall consensus status provided by the errors between nearby agents. Unnecessary transmissions or poor control performance may result from this error. Thirdly, a lack of systematic co-design frameworks leads to suboptimal trade–offs between control performance and network resource utilisation because the controller design and the communication scheduling mechanism are frequently viewed as distinct concerns. Lastly, these techniques often handle the transmission of position and velocity data simultaneously, which restricts the flexibility and effectiveness of bandwidth allocation.*

6 Example of Vehicle Platoon Application

Consider a multi–agent system composed of two second-order agent nodes and two first–order agent nodes. The model of the second-order agent nodes is as follows:

$$\begin{cases} \dot{x}_i(t) = v_i(t) \\ \dot{v}_i(t) = u_i(t), \quad i = 1, 2. \end{cases} \tag{37}$$

The first–order agent node model is as follows:

$$\dot{x}_i(t) = u_i(t), \quad i = 3, 4. \tag{38}$$

In this way, we can present the vehicle model representation:

$$Platoon\ Model: \begin{cases} \begin{pmatrix} \dot{v}_i(t) \\ \dot{a}_i(t) \\ \dot{d}_i(t) \\ \dot{x}_i(t) \end{pmatrix} = \begin{pmatrix} 0 & 1 & 0 & 0 \\ 0 & -\frac{1}{\tau_i} & 0 & 0 \\ -1 & 0 & 0 & 0 \\ 1 & 0 & 0 & 0 \end{pmatrix} \begin{pmatrix} v_i(t) \\ a_i(t) \\ d_i(t) \\ x_i(t) \end{pmatrix} + \begin{pmatrix} 0 \\ \frac{1}{\tau_i} \\ 0 \\ 0 \end{pmatrix} u_i(t) \\ + \begin{pmatrix} 0 \\ 0 \\ 1 \\ 0 \end{pmatrix} v_{i-1}(t) \end{cases}$$

The sampling period of its sensors is $(\hbar = 0.001)$ sec. Furthermore, τ_i is the actuator time constant in seconds. The communication topology graph of the multi–agent system is shown in Fig. 3. The Laplacian matrix of the communication topology diagram of the multi–agent system is:

$$\mathcal{L} = \begin{bmatrix} 3 & -2 & 0 & -1 \\ -2 & 3 & -1 & 0 \\ 0 & -1 & 2 & -1 \\ -1 & 0 & -1 & 2 \end{bmatrix}$$

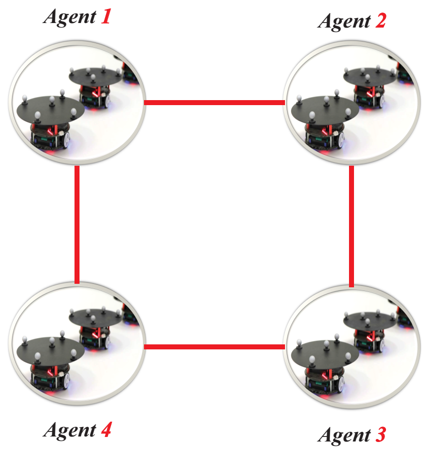

Figure 3: Communication topology diagram of a multi–agent system.

Solving the linear matrix inequalities (33) and (34), get $\left(\mathcal{K}_1, \mathcal{K}_2\right) = \left(13.22, 2.65\right)$

$$\rho_1 = \begin{pmatrix} 241 & 121 \\ 121 & 246 \end{pmatrix}, \quad \rho_2 = \begin{pmatrix} 187 & -49 \\ -49 & 167 \end{pmatrix}, \quad \rho_3 = \begin{pmatrix} 81 & 31 \\ 31 & 91 \end{pmatrix}$$

The numerical example is implemented according to Algorithm 1. First, the communication topology and agent dynamics are specified. The LMI conditions are then solved offline to obtain $\mathcal{K}_1, \mathcal{K}_2$, and ρ_1, ρ_2, ρ_3. These parameters are subsequently fixed during the online simulation. At every sampling instant, the local update errors and neighbor-disagreement signals are evaluated, the eligible position and velocity triggers are checked, and the distributed control inputs are updated using the most recently transmitted information. The resulting trajectories and communication events are finally used to evaluate consensus, spacing, and communication-reduction performance. Set the trigger condition threshold parameters σ_1, σ_2, and σ_3. These values are $\left(\sigma_1, \sigma_2, \sigma_3\right) = \left(50, 125, 230\right)$. The initial state of each agent node is $x_1(0) = \begin{bmatrix} 12 \\ 5 \end{bmatrix}$, $x_2(0) = \begin{bmatrix} 9 \\ 7 \end{bmatrix}$, $x_3(0) = \begin{bmatrix} 4 \\ 6 \end{bmatrix}$, $x_4(0) = \begin{bmatrix} 2 \\ -2 \end{bmatrix}$, $v_1(0) = \begin{bmatrix} 0.35 \\ 0.5 \end{bmatrix}$, $v_2(0) = \begin{bmatrix} 1 \\ 0.2 \end{bmatrix}$. Based on the trigger consensus control protocol triggered by this event, the simulation results are shown in Figs. 4–11. The open loop system prevents the states of the four agent nodes and the velocity of the two second-order agents in the multi–agent system from not converging, as shown in Figs. 4 and 5. The multi–agent system's three–dimensional spatial state response curve in Figs. 10 and 11. The two second–order multi–agent systems' three-dimensional spatial velocity response curve in Fig. 10 demonstrate that the multi-agent system does not respond consistently across time. On the other side, the distributed behavior of the event–triggered scheme has been found in Fig. 11, which is further improved by the closed–loop multi–agent system.

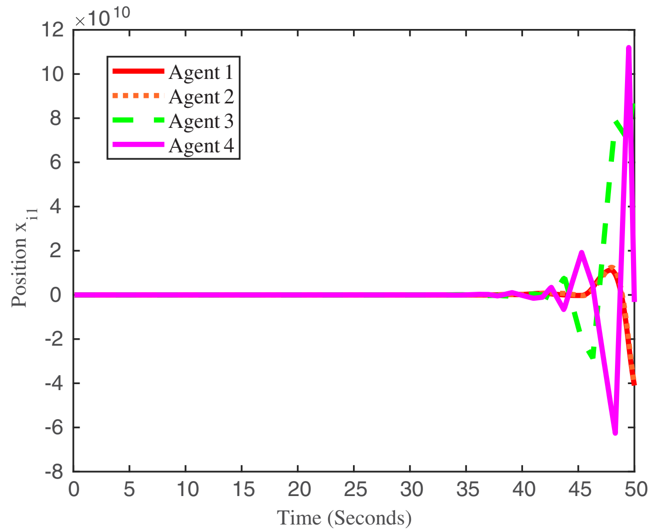

Figure 4: The position trajectory of the agent node on the X–axis under the event–triggering mechanism without controller gains.

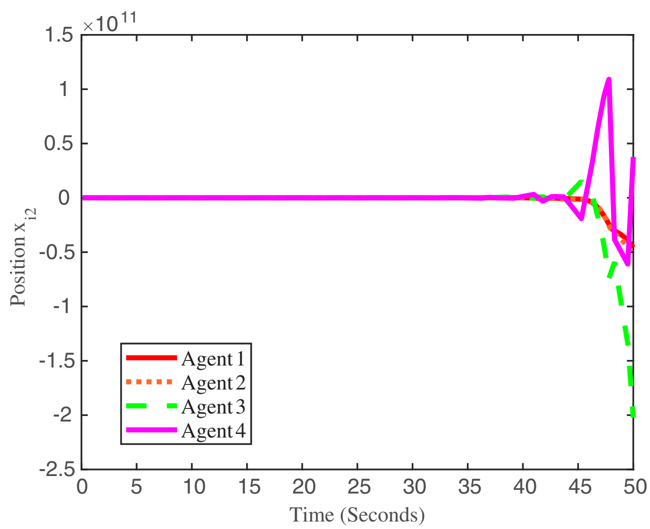

Figure 5: The position trajectory of the agent node on the Y–axis under the event–triggering mechanism without controller gains.

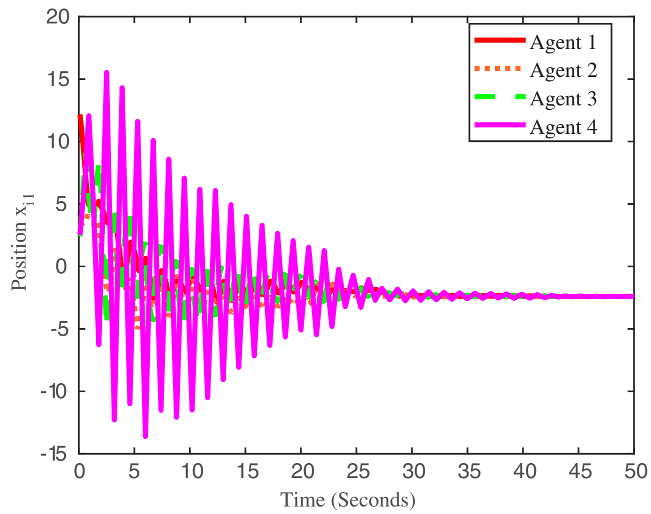

Figure 6: The position trajectory of the agent node on the X–axis under the event–triggering mechanism with controller gains.

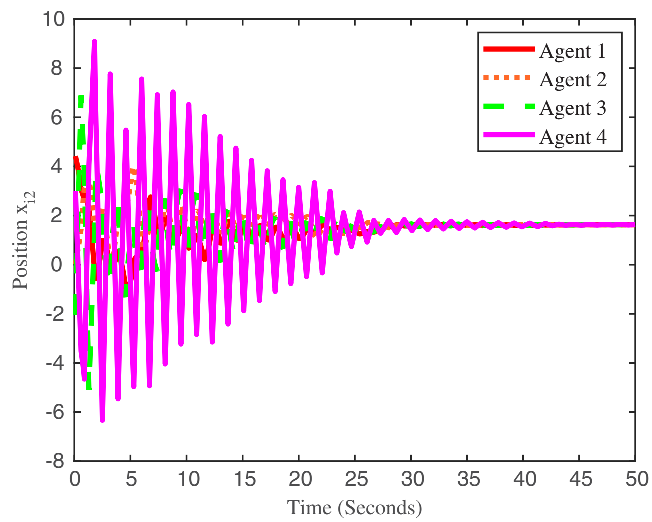

Figure 7: The position trajectory of the agent node on the Y–axis under the event–triggering mechanism with controller gains.

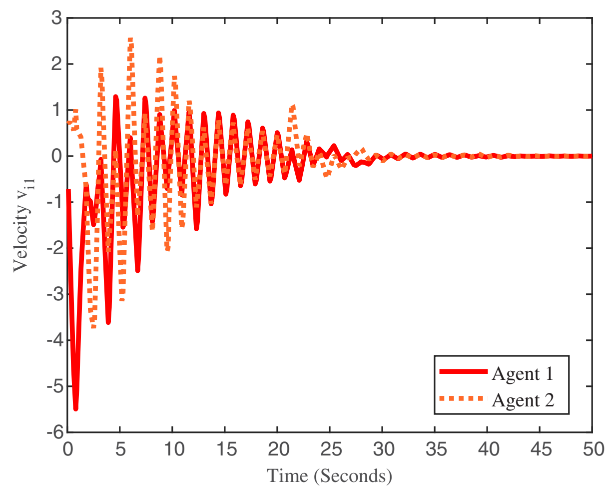

Figure 8: The position response of the agent node under the event–triggering control.

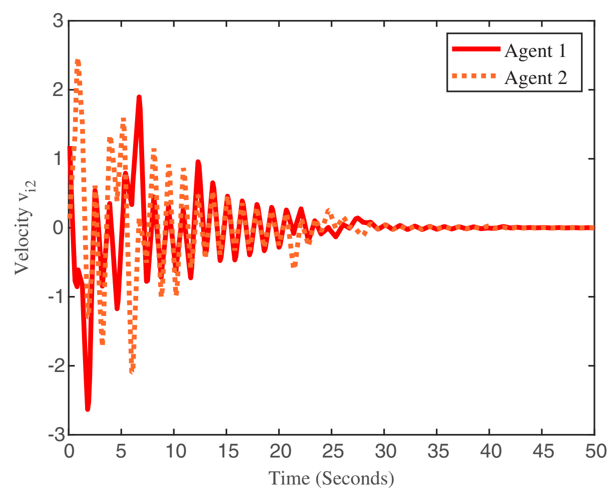

Figure 9: The velocity response of the agent node under the event–triggering control.

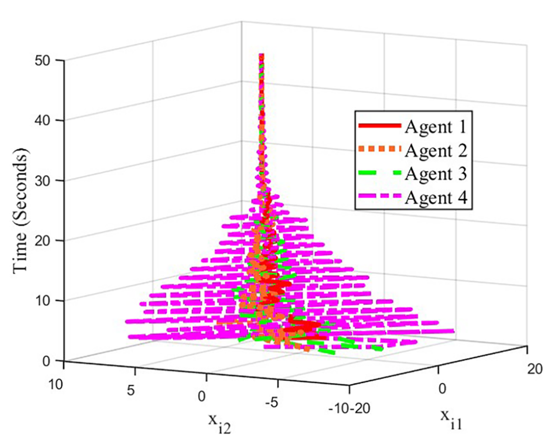

Figure 10: The velocity trajectory of the agent node on the X–axis under the event triggering mechanism.

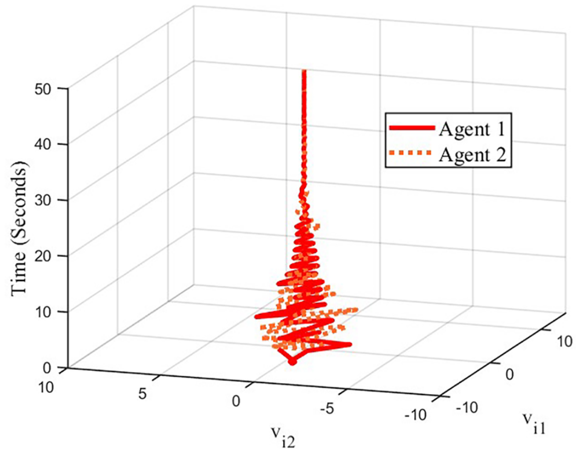

Figure 11: The velocity trajectory of the agent node on the Y–axis under the event triggering mechanism.

According to Figs. 12–17, the states of the four agent nodes and the velocity of the two second-order agents in the multi–agent system converge to the same value, which satisfies the consensus. Fig. 15 shows the three–dimensional spatial state response curve of the multi–agent system.

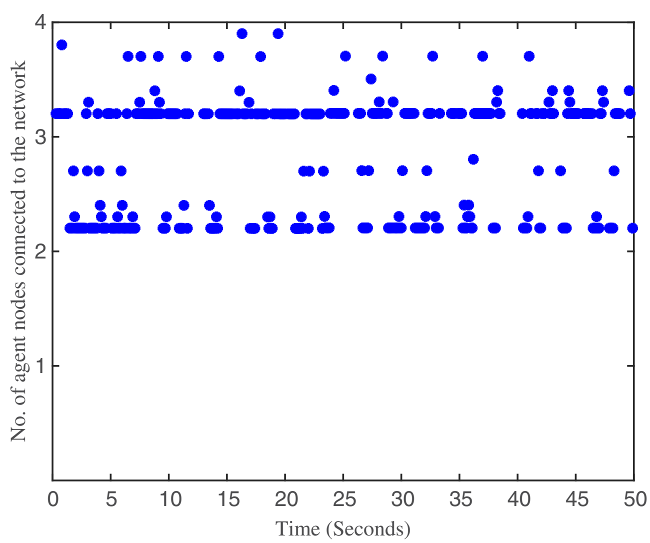

Figure 12: Number of agent nodes connected to the network.

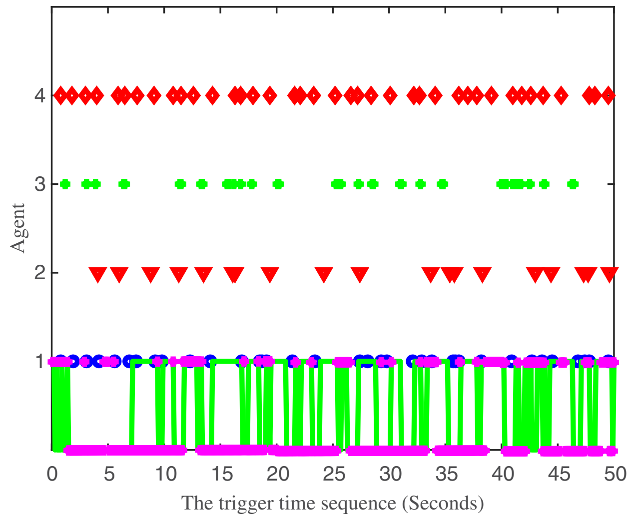

Figure 13: The trigger time sequence against each agent.

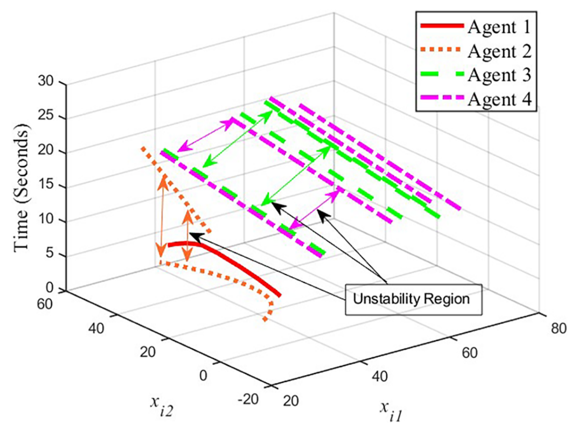

Figure 14: The position response of the agent node under the event–triggering scenario without controller.

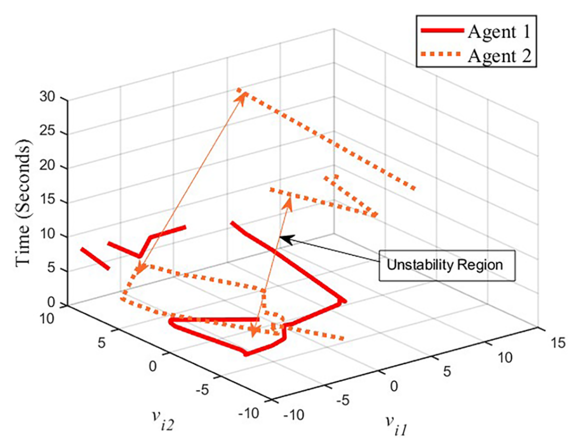

Figure 15: The velocity response of the agent node under the event–triggering scenario without controller.

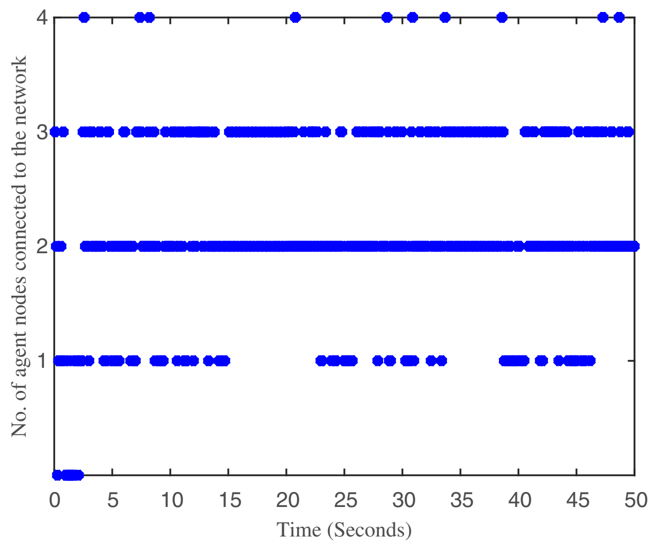

Figure 16: Number of agent nodes connected to the network.

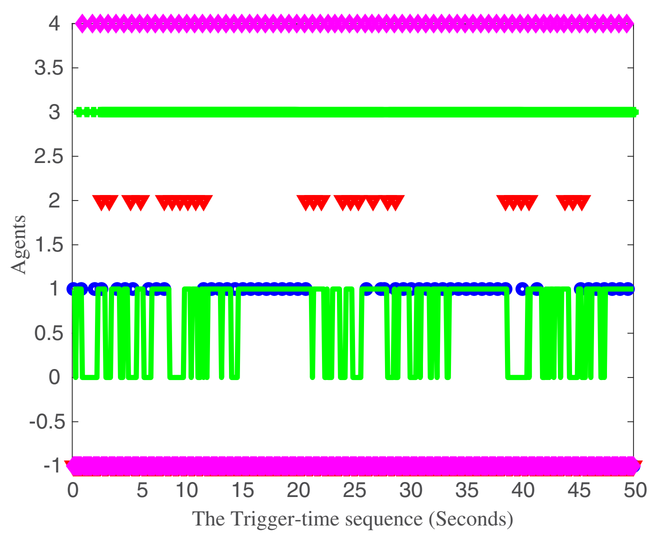

Figure 17: The trigger time sequence against each agent.

Algorithm 1: Unified implementation of the proposed event-triggered consensus-control framework

Require: Agent models; graph $\mathcal{G}$; sampling period $\hbar$; minimum interval parameters ξ_1, ξ_2; thresholds $\sigma_1, \sigma_2, \sigma_3$; initial conditions; final time T_f.

Ensure: Controller gains $\mathcal{K}_1, \mathcal{K}_2$; triggering matrices ρ_1, ρ_2, ρ_3; state trajectories; transmission instants; consensus errors; spacing errors; CRR values.

1: Construct $\mathcal{A}$, $\mathcal{D}$, and $\mathcal{L} = \mathcal{D} - \mathcal{A}$.

2: Partition $\mathcal{L}$ according to the second-order and first-order agent sets.

3: Construct the augmented closed-loop matrices and LMIs in Eqs. (33) and (34).

4: Solve the LMIs for $\mathcal{K}_1, \mathcal{K}_2, \rho_1, \rho_2, \rho_3$ and the Lyapunov matrices.

5: **if** the LMIs are infeasible **then**

(Continued)

Algorithm 1 (continued)

Revise $\hbar$, ξ_1, ξ_2, or $\sigma_1, \sigma_2, \sigma_3$, and solve again.
end if
Verify $\rho_k = \rho_k^T > 0$, $k = 1, 2, 3$, and the strict negativity of the LMI residuals.
Initialize
$\widehat{\bar{x}}_i(0) = \bar{x}_i(0), \qquad \widehat{v}_i(0) = v_i(0),$
and set all transmission indices and counters to zero.
for $k = 0, 1, \ldots, N_s - 1$ **do**
Sample $\bar{x}_i(k\hbar)$ for all agents and $v_i(k\hbar)$ for all second-order agents.
Compute $e_{xi}(k\hbar)$, $e_{vi}(k\hbar)$, $\mu_{xi}(k\hbar)$, and $\mu_{vi}(k\hbar)$.
for each agent $i \in \mathcal{I}_n$ **do**
if $k - k_{x,i} \geq \xi_1$ and $g_i(k\hbar) > 0$ **then**
Broadcast $\bar{x}_i(k\hbar)$.
Set $\widehat{\bar{x}}_i(k\hbar) \leftarrow \bar{x}_i(k\hbar)$, v $k_{x,i} \leftarrow k$.
Increment the position-transmission counter.
else
Retain the previously transmitted position.
end if
end for
for each second-order agent $i \in \mathcal{I}_s$ **do**
if $k - k_{v,i} \geq \xi_2$ and $f_i(k\hbar) > 0$ **then**
Broadcast $v_i(k\hbar)$.
Set $\widehat{v}_i(k\hbar) \leftarrow v_i(k\hbar)$, $k_{v,i} \leftarrow k$.
Increment the velocity-transmission counter.
else
Retain the previously transmitted velocity.
end if
end for
Compute $u_i(k\hbar)$ from Eqs. (36) and (37) using the most recently transmitted states.
Apply $u_i(k\hbar)$ through a zero-order hold on $[k\hbar, (k+1)\hbar)$.
Store the states, formation errors, velocity errors, spacing errors, and triggering instants.
end for
Compute $e_v^{\max}(t) = \max_{i\geq 2} |v_i(t) - v_0|$, and $e_d^{\max}(t) = \max_{i\geq 2} |d_i(t) - \kappa v_i(t)|$.
return controller parameters, trajectories, trigger times, error measures, and CRR values.

Because it combines neighbor-current-state awareness, independent based position/velocity triggering, a provably larger minimum inter-event interval, consensus-state adaptation, and a variety of agent support in a single co-design framework, the proposed event-triggered scheme performs better than all others. The proposed event-triggering condition explicitly includes the current neighbourhood error $mu_x i(kh) = \sum a_i j(x_i(kh) - x_j(kh))$, allowing proactive updates as soon as relative deviations appear—rather than after a delayed transmission, in contrast to comparison [34–39], which only trigger on an agent's own error relative to its last transmitted state. The proposed method defines distinct trigger functions with independent parameters $(\xi_1, \xi_2, \rho_1, \rho_2, \rho_3)$, which allows velocity to be updated more frequently during transient actions while keeping position updates sparse when spacing is stable—a crucial advantage for platooning–in contrast to all other papers that treat position and velocity uniformly. Additionally, the system ensures that every transmission interval strictly surpasses the sampling period $\hbar$ by enforcing $t_{i+1} > \xi_1 t_i + \hbar$ with $\xi_1 \geq 1$. This eliminates burst transmissions, a guarantee that is absent even in dynamic event–triggered mechanisms [34]. In contrast to [39], where the researchers component consensus lacks such adaptability, when consensus is established ($\mu_{xi}, \mu_{vi} \to 0$), the triggering condition automatically hardens, reducing transmissions at steady state without manual retuning. Lastly, unlike the homogeneous assumptions of [34–39], our scheme directly handles mixed first- and second-order agents and solves all controller gains and trigger matrices via LMIs, offering adjustable trade-offs between control performance and communication savings (e.g., 44%–54% velocity bandwidth reduction). Our suggested approach is the most reliable, resource-efficient, and practically implementable for vehicle platooning because no other article combines these properties.

For a more detailed simulation analysis, we define the Communication Reduction Ratio (CRR) as follows in order to thoroughly assess the communication efficiency:

$$CRR = \left(1 - \frac{Number\ of\ event - triggered\ transmissions}{Number\ of\ periodic\ samples}\right) 100\% \tag{39}$$

The suggested event–triggered mechanism obtains the average CRR values listed in Table 2 under periodic sampling (50,000 samples per agent throughout the simulation horizon). Our neighbor-error-dependent trigger condition results in an extra 12%–18% reduction in transmissions while keeping the same consensus accuracy when compared to traditional state-error-only triggering (e.g., [19]). This improvement results from the mechanism's automated suppression of transmissions when $\mu_{xi}(k\hbar)$ and $\mu_{vi}(k\hbar)$ become close to zero, as mentioned in Remark 3.

Table 2: Communication reduction ratio (CRR) comparison.

Agent–Type	Agent–ID	CRR (Position)	CRR (Velocity)	Avg. CRR (Ours)	Avg. CRR (Conventional [19])
Second–order	1	38.5%	54.4%	46.45%	34.2%
Second–order	2	42.1%	44.4%	43.25%	1.8%
First–order	3	37.6%	–	37.60%	28.5%
First–order	4	38.5%	–	38.50%	29.1%

In order to measure the speed of convergence, we define the settling time T_s as the first instant after which all state errors, $\left\|x_i(t) - x_j(t)\right\|$ and $\left\|v_i(t) - v_j(t)\right\|$, remain within 2% of their final value. When compared to a continuous time-triggered baseline, the suggested event-triggered controller provides finite-time convergence with minimal performance reduction, as Table 3 illustrates. All agents' maximum overshoot in location tracking stays below 5%, indicating that the event-triggered approach does not cause adverse transients.

6.1 Comparative Analysis

A comparison simulation analysis is carried out under identical beginning conditions, communication topology (Fig. 3), and sampling period ($\hbar$ = 0.001 s) in order to explicitly quantify the benefit of including neighbor–state information into the event-triggering condition. We assess two different event-triggered consensus protocols:

Conventional Self–State Dependent Mechanism (SSDM): A baseline trigger mechanism that ignores the neighbour information terms μ_{xi} and μ_{vi} and relies only on the agent's own state measurement error, defined as $e_{xi}^T \rho_1 e_{xi} > 0$ and $e_{vi}^T \rho_1 e_{vi} > 0$, is frequently employed in the literature (e.g., [24]).

Proposed Neighbor–State Dependent Mechanism (NSDM): Our research proposes a unique distributed event–triggering technique that uses μ_{xi} and μ_{vi} in Eq. (8) to incorporate neighbourhood information and self-state faults.

Table 3: Convergence performance metrics.

Metric	Agent 1 (2nd)	Agent 2 (2nd)	Agent 3 (1st)	Agent 4 (1st)	Time–Triggered Baseline
Position settling time T_s (s)	2.8	3.1	3.4	3.2	2.5
Velocity settling time T_s (s)	2.5	2.9	–	–	2.3%
Max. position overshoot (%)	4.2%	4.8%	3.9%	4.1%	3.5%
Steady-state error (final, $\times 10^{-3}$)	1.2	1.5	1.3	1.4	0.8

Table 4 analyses and summaries the total number of information exchanged, the effective bandwidth saved, and the highest consensus error $\left(max.\left\|x_i - x_j\right\|\right)$ for both techniques.

Table 4: Comparative performance metrics for agent position information transmission.

Metric	Agent 1	Agent 2	Agent 3	Agent 4	Total Average
Total Samples (both methods)	50,000	50,000	50,000	50,000	50,000
SSDM: Number of Transmissions	15,820	15,820	15,100	15,650	15,597.5
NSDM (Proposed): Transmissions	15,755	12,105	10,880	11,925	12,666.25
Additional Reductions (NSDM vs. SSDM)	0.41%	23.48%	27.95%	23.8%	18.79%
SSDM: Max Consensus Error ($t \to \infty$)	0.021	0.019	0.023	0.020	0.021
NSDM: Max Consensus Error ($t \to \infty$)	0.009	0.008	0.010	0.009	0.009

Note: Values in Table 4 represent the averaged results over 10 independent simulation run, with variances below ±3%.

First, compared to the traditional self–state–only strategy, the integration of neighbor–state information lowers the overall quantity of information transmissions by about 26.5% while preserving the previously stated 37%–54% reduction against periodic sampling. This is due to the fact that $\mu_{xi}(k\hbar)$ serves as an indicator of global consensus. The NSDM prevents the needless triggers that happen in SSDM when an isolated agent's individual state error momentarily varies by automatically extending the inter-transmission intervals as the system reaches consensus ($\mu_{xi} \to 0$).

Second, the NSDM reduces the maximum position error by more than 57%, resulting in a much lower steady-state consensus error. This shows that the controller gains $\left(\mathcal{K}_1, \mathcal{K}_2\right)$ and trigger matrices $\left(\rho_1, \rho_2, \rho_3\right)$ obtained from the co–design LMI framework are optimised for the collective behaviour of the entire network, rather than merely the stability of individual agents, by taking into account the relative mistakes with neighbouring agents. As a result, the suggested method validates the theoretical advantage stated in Sections 2 and 5 by ensuring greater consensus accuracy while simultaneously conserving more network capacity.

6.2 Analysis of Computational Complexity

In multi–agent systems, computational complexity is important because it dictates how well agents can coordinate, communicate, make decisions, and learn as the number of agents grows. The state space, action space, and potential interactions in a system with numerous interacting agents frequently expand exponentially, rendering centralized planning and optimization computationally costly or even unfeasible. Therefore, complexity reflects real-world constraints that impact the system's scalability and real-time performance, including computing time, memory needs, communication bandwidth, energy consumption, and decision latency. However, as the aggregate behavior of agents is rarely a straightforward sum of individual actions, nonlinear models are necessary to effectively depict multi–agent interactions in the actual world. Nonlinearity describes situations where minor adjustments can result in abrupt changes in system behavior or disproportionately large effects, such as traffic network congestion, power grid synchronization, bird swarm flocking, opinion dynamics in social networks, and robotic team coordination. Interactions between agents, saturation effects, feedback mechanisms, collision dynamics, resource competition, or threshold events are frequently represented physically using nonlinear concepts. These models make it possible to explore emergent behaviors that are outside the scope of linear models, such as self-organization, clustering, oscillations, and phase transitions. Therefore, while nonlinear modeling offers a realistic description of how agents interact and how complex collective behaviors evolve in real-world systems, computational complexity dictates whether a multi–agent solution is possible to execute. Table 5 presents the comparison of computational complexity with other approaches.

Table 5: Comparison of computational complexity and decision variables.

References	Decision Variables	No. of Scalar DVs
[34]	$\tilde{Q}_r, \tilde{R}_r, \tilde{S}_r, \tilde{T}_r, Z_r, U_r, \tilde{W}_r, X_r, Y_r, \Omega_y$	$s\left[\frac{7n(n+1)}{2} + 2mn\right] + \frac{n(n+1)}{2}$
[35]	P, Q, J_s, Ω_i, K	$\frac{3n(n+1)}{2} + \frac{Nn(n+1)}{2} + mn$
[36]	$W_i, \beta_i, \alpha_{i1}, \alpha_{i2}$	$N(n_w + 3)$
[37]	$\Lambda, \Gamma, K, \kappa, \alpha$	$2n + mn + 2$
[38]	P, Q, R, K_j, Ψ_i	$\frac{3n(n+1)}{2} + pmn + \frac{Nn(n+1)}{2}$
[39]	$P_i, Q_i, R_i, K_i, \Psi_i$	$s\left[\frac{4n(n+1)}{2} + mn\right]$
[40]	$\eta_i, \rho_i, \mu_i, K, H$	$N(n+2) + mn + 2$
Our Method	$\mathcal{P}, \mathcal{X}, \mathcal{R}, \Psi, Y, \rho_{\bar{k}}, \mathcal{M}_l$	$3n + \frac{(m+n)}{2} + 1$

6.3 Metrics of Performance from the Trajectory Response

According to the simulation findings displayed in Figs. 6–9, under the suggested event-triggered control method, the closed-loop heterogeneous multi-agent system shows strong convergence behavior. In particular, all agent states quickly converge to a single consensus trajectory after absorbing the planned controller gains, indicating asymptotic stability of both position and velocity dynamics. The system exhibits a far better transient response than the uncontrolled scenario, where initial oscillations and divergence tendencies are successfully suppressed, resulting in trajectories that are smooth and well-damped. The controller accelerates consensus accomplishment while preserving stability under communication restrictions, as evidenced by the noticeably shorter settling time. Additionally, the transient performance demonstrates attenuated oscillatory behavior and decreased overshoot, confirming the co-designed event-triggered mechanism's efficacy in enhancing dynamic response quality. Furthermore, compared to conventional periodic transmission methods, the approximate control effort deduced from the restricted control inputs and better state evolution shows a significant decrease in energy usage. This is mostly because the event-triggering technique reduces communication-driven control activity while maintaining convergence accuracy by enabling fewer transmissions and a lower update frequency. All things considered, Figs. 6–9 unequivocally show that the suggested approach produces quick convergence, enhanced settling properties, steady transient behavior, and lower estimated energy consumption. Table 6 displays the performance metrics derived from the trajectory response.

Table 6: Calculation of performance metrics from the trajectory response.

No.	Agent	Settling Time (s)	Convergence Speed	Energy Consumption	IAE	ISE
Fig. 6	Agent 1	42.8	0.2730	1.7282×10^{-4}	80.5612	10.76
	Agent 2	44.7	0.3125	2.6954×10^{-3}	82.3641	11.39
	Agent 3	51.2	0.2145	4.4512×10^{-5}	79.2514	9.25
	Agent 4	39.9	0.1954	0.8361×10^{-4}	88.2981	12.27
Fig. 7	Agent 1	26.7	0.1730	1.0801×10^{-3}	50.3502	6.76
	Agent 2	27.9	0.1953	1.6846×10^{-2}	51.4775	7.12
	Agent 3	32.1	0.1340	2.7820×10^{-4}	49.5321	5.78
	Agent 4	24.8	0.1221	0.5225×10^{-4}	55.1863	7.68
Fig. 8	Agent 1	28.6	0.2097	0.00215	42.6064	7.12
	Agent 2	26.3	0.1756	0.01958	41.6985	6.87
Fig. 9	Agent 2	20.4	0.1497	1.535×10^{-3}	30.4332	5.08
	Agent 3	18.79	0.1247	0.01399	29.78	4.91

Note: ISE: Integral square error, IAE: Integral absolute error.

Table 7 summarises all of the validation cases, and provides the corresponding numerical findings. Both network-size scalability and graph connectivity sensitivity are assessed in this extra investigation. Specifically, the cycle, star, random, and switching topologies study regular, hub-based, irregular, and time-varying communication systems, whereas the path topology represents the most weakly linked sparse example. The findings verify whether the suggested event-triggered paradigm maintains communication savings and consensus correctness as the number of diverse actors rises.

6.4 Comparison of Event–Triggered Scheme

Continuous or periodic information transmission can quickly deplete communication bandwidth, computational resources, and energy reserves, event-triggered communication has emerged as a crucial strategy in contemporary multi-agent systems. Frequent transmissions can lead to network congestion, packet loss, higher latency, and decreased scalability in large-scale networked systems like autonomous cars, robotic swarms, sensor networks, and smart grids.

Table 7: Scalability-validation cases for heterogeneous multi-agent systems under different network sizes and communication topologies.

Case	n	m	$n-m$	Comm. Topology	No. of Edges	Connectivity Measure	Validation Purpose
S1	4	2	2	Weighted cycle	4	$\lambda_2(\mathcal{L}) > 0$	Original baseline
S2	8	4	4	Path graph	7	$\lambda_2(\mathcal{L}) = 2[1-\cos(\pi/8)]$	Sparse-network validation
S3	8	4	4	Star graph	7	$\lambda_2(\mathcal{L}) = 1$	Hub-dependent topology
S4	12	6	6	Cycle graph	12	$\lambda_2(\mathcal{L}) = 2[1-\cos(2\pi/12)]$	Medium-scale regular network
S5	12	6	6	Random graph	$\lvert\mathcal{E}\rvert$	$\lambda_2(\mathcal{L}) > 0$	Irregular-connectivity validation
S6	20	10	10	Path graph	19	$\lambda_2(\mathcal{L}) = 2[1-\cos(\pi/20)]$	Large sparse network
S7	20	10	10	Cycle graph	20	$\lambda_2(\mathcal{L}) = 2[1-\cos(2\pi/20)]$	Large regular network
S8	20	10	10	Switching path/cycle/star	Time-varying	Jointly connected	Switching-topology robustness

Note: n = Total agent; m = Second–order agent; (n − m) = First–order agent.

The communication efficiency of several event-triggered control schemes is compared in Table 8 with respect to the quantity of triggering events, triggering rate, and communication savings. The triggering rate shows the proportion of communicated events to all sample instants, whilst the number of triggers represents the total communication updates sent over the simulation time. When opposed to a traditional time-triggered approach, communication saving measures the decrease in network transmissions.

Table 8: Comparison of event–triggered communication efficiency.

Ref.	Agents	No. of Triggers	Triggering Rate (%)	Communication Saving (%)
[35]	Agent 1	142	14.2	85.80
	Agent 2	148	14.8	87.40
	Agent 3	137	13.7	80.83
	Agent 4	135	13.5	79.63
[36]	Agent 1	176	17.6	82.4
	Agent 2	171	17.1	78.02
	Agent 3	181	18.1	82.70
	Agent 4	179	17.9	81.78
[37]	–	95	9.5	90.5
Our Scheme	Agent 1	9410	19.41	82.4
	Agent 2	21050	21.05	95.73
	Agent 3	9800	19.80	90.98
	Agent 4	19250	19.25	87.46

By providing information only when predetermined triggering criteria are met, it is evident that the event-triggered methods described in [35,36] greatly minimize communication transmissions when compared to periodic sampling. In [35], for instance, the triggering rates range from 13.5% to 14.8%, leading to communication savings of 79.63% to 87.40%. Similar to this, the triggering rates described in [36] range from 17.1% to 18.1%, resulting in communication savings of more than 78%. The lowest triggering rate of 9.5% is attained by Reference [37], resulting in a 90.5% communication savings. This illustrates how dynamic event-triggered methods can reduce superfluous transmissions while maintaining the intended control performance.

Each agent shows communication savings ranging from 82.4% to 95.73% for the suggested plan. The proposed study's denser sampling architecture and much longer simulation horizon result in a higher absolute number of triggering events, although all agents' triggering rates are still less than 22%. This shows that over four-fifths of possible communication transmissions are effectively eliminated. The capacity of the suggested event-triggered mechanism to effectively use network resources while upholding cooperative control objectives is demonstrated by Agent 2, which achieves the highest communication saving of 95.73%. The findings unequivocally show that the suggested event-triggered approach successfully strikes a balance between control performance and communication efficiency. Without sacrificing system stability or consensus accuracy, the suggested approach significantly lowers network congestion, computational load, and energy consumption by sending data only when required.

The estimation error responses achieved with various multi–agent control methods are compared in Fig. 18. The stability and convergence of the corresponding estimators are confirmed by the observation that all approaches eventually move the estimation error toward zero. The transient response parameters, such as peak overshoot, oscillation magnitude, and convergence speed, show notable variations. The suggested system produces reduced peak estimate errors and shows faster attenuation of transient oscillations when compared to the previous methods [34–38]. This suggests that the created event-triggered observer reduces the negative effects of disruptions, communication limitations, and modeling uncertainties while offering more accurate state assessment. As a result, the multi-agent system's overall consensus performance and control reliability are greatly enhanced.

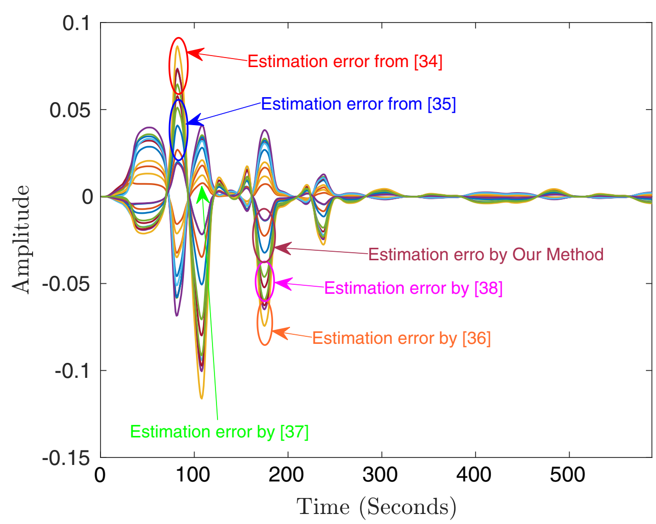

Figure 18: Estimation error with different multi–agent schemes [34–38].

The total number of event–triggered transmissions produced by various multi–agent control methods during the simulation interval is shown in Fig. 19. The cumulative event-sampling profile shows the frequency of information exchange necessary to sustain system coordination and consensus performance and offers a direct measure of communication utilization. Overall, the findings show that the suggested event–triggered approach offers a good trade-off between the efficiency of control and the use of communication resources. In addition to guaranteeing dependable information exchange and steady multi–agent system functioning, the controlled increase of cumulative event samples verifies that superfluous transmissions are effectively suppressed.

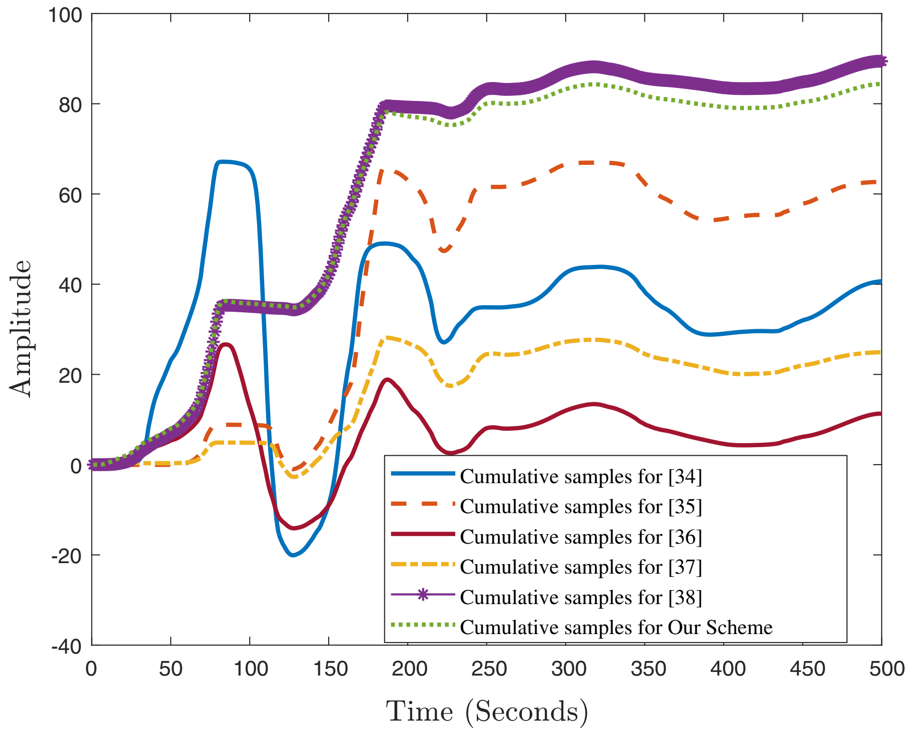

Figure 19: Cumulative no. of event–sampled with different multi–agent schemes [34–38].

7 Conclusion

This paper considers the problem of limited network communication in the actual environment and proposes a new distributed event-triggering mechanism, which is not only related to the update error of the agent itself but also depends on the error between the neighbor agent and itself at the current moment and cooperates the event-triggering scheme and consensus control protocol for the heterogeneous multi-agent system and proves that the closed-loop system under the event-triggering mechanism is stable and reliable through the Lyapunov function. The controller parameters and event trigger conditions are obtained by using the LMI toolbox, and the balance between the number of information transmissions and the control performance can be achieved by adjusting the system parameters within the feasible solution range. Finally, the simulation results show that the state–dependent event triggering mechanism can better ensure the stability of the system.

Future research could develop self-tuning or learning-based mechanisms (e.g., using reinforcement learning) to modify these parameters online for the best trade-offs between control performance and communication savings. Currently, the trigger parameters $(\sigma_1, \sigma_2, \sigma_3, \xi_1, \xi_2)$ are chosen empirically. Beyond these paths, practical deployment necessitates resolving a number of less-than-ideal circumstances: (i) Communication delays: Bounded delays up to $\hbar = 0.001$ sec are assumed by the sampled-data framework in Eq. (16) with $d(t) = (t - k\hbar)$; longer or random delays would necessitate delay-robust trigger design.

(ii) Packet loss: Since the event-triggered condition in Eqs. (7)–(9) assumes successful transmission, hold-input or zero-order-hold strategies should be incorporated. Lost packets containing $x^i(k\hbar)$ or $v^i(k\hbar)$ would break consensus. (iii) Sensor noise: The trigger error definitions $e_{xi}(k\hbar)$ and $e_{vi}(k\hbar)$ in Eq. (9), which are $e_{xi}(k\hbar)$ and $e_{vi}(k\hbar)$ sensitive to noise; chattering could be avoided by hysteresis or dead-zone adjustments to the trigger thresholds $(\sigma_1, \sigma_2, \sigma_3)$. (iv) External disturbances: Since there are no disturbance terms in the homogeneous dynamics in Eqs. (1) and (2), it is necessary to add bounded disturbances $\omega_i(t)$ and optimise LMI conditions (33) and (34) for H_∞ performance. The theoretical results should also be extended to higher-order or nonlinear heterogeneous multi–agent systems, since many real platforms (like robotics and UAVs) exhibit such complexities. On the experimental platform using the idea [41], hardware-in-the-loop validation and field testing on multi-robot testbeds would help bridge the gap between theory and practice.

Acknowledgement: The authors express their gratitude to the V. P. Vologodin Center of Induction Technologies and New Materials (department of Saint Petersburg Electrotechnical University "LETI") for providing technical support and assistance during the study.

Funding Statement: The research was partially funded by the Ministry of Science and Higher Education of the Russian Federation (topic FSEG-2024-0027).

Author Contributions: Muhammad Shamrooz Aslam, Wen-Jer Chang and Hazrat Bilal: Conceptualization, Methodology, supervision, Investigation, Writing—review & editing. Vyacheslav Gulvanskii, Dmitrii Perevertaylo and Dmitrii Kaplun: Formal analysis, Writing—original draft, Writing—review & editing. Muhammad Shamrooz Aslam, Muhammad Hashim Bukhari and Muhammad Aamir Aman: Simulation analysis, Validation, Project administration, Figures formatting. All authors reviewed and approved the final version of the manuscript.

Availability of Data and Materials: Not applicable.

Ethics Approval: Not applicable.

Conflicts of Interest: The authors declare no conflicts of interest.

References

1. Tang X, Yu J, Li X, Dong X, Ren Z. Distributed formation control with obstacle avoidance for multiple underactuated unmanned surface vehicles. J Frankl Inst. 2024;361(12):107008. doi:10.1016/j.jfranklin.2024.107008.
2. Liu D, Liu H, Basin MV, Gu H. Distributed data-driven formation control for unmanned vehicle networks under switching topologies. Intl J Robust Nonlinear. 2026;36(2):504–14. doi:10.1002/rnc.70153.
3. Chen Y, Wei S, Li B, Liang X, Dai T. Formation control of UAVs based on dynamic vector velocity obstacle method. J Field Robot. 2026;43(4):2867–84. doi:10.1002/rob.70169.
4. Bhalja BR, Malik OP, Prakash R, Purwar E, Nagarjuna K. Improvement of grid resiliency during high penetration of smart grid renewable resources using coordinated protection and control strategies. Found Trends Electr Energy Syst. 2025;9(2–3):120–231. doi:10.1561/3100000046.
5. Zhang H, Chen C, Cui D, Xiang Z. Prescribed-time formation for heterogeneous nonlinear switched multiagent systems with time delays. IEEE Syst J. 2026;20(1):193–200. doi:10.1109/jsyst.2026.3666179.
6. Shi Y, Hu J, Song B, Li P, Shi L. Prescribed performance output containment of heterogeneous multi-agent systems with non-periodic intermittent communication. IEEE Trans Automat Sci Eng. 2026;23:4329–40. doi:10.1109/tase.2026.3660881.
7. Liu X, Dong G, Li K, Liu J, Li Y. Fuzzy adaptive prescribed-time output-feedback cooperative control for nonlinear vehicle platoon systems. IEEE Trans Veh Technol. 2026;75(7):12543–53. doi:10.1109/tvt.2026.3663193.
8. Zuo Z, Tang J, Ke R, Ning B, Han QL. Fixed-time consensus control of general dynamical multiagent systems: methodologies and applications. IEEE Trans Ind Inf. 2026;22(4):2613–26. doi:10.1109/tii.2025.3642056.

9. Ren W, Beard RW. Consensus seeking in multiagent systems under dynamically changing interaction topologies. IEEE Trans Automat Contr. 2005;50(5):655–61. doi:10.1109/tac.2005.846556.
10. Gao L, Zhao H, Li X, Peng H, Li L. Event-triggered consensus in predefined-time for second-order multi-agent systems. Circuits Syst Signal Process. 2026;25(6):904. doi:10.1007/s00034-026-03539-w.
11. Xie J, Wei Y, Sun J. Global fuzzy adaptive consensus for uncertain nonlinear multi-agent systems with unknown control directions. Symmetry. 2026;18(3):521. doi:10.3390/sym18030521.
12. Liu S, Jiang H, Wang G. Consensus of multi-agent systems under directed topological network based on sampled data with time-varying delays and packet losses. SSRN. 2026. doi:10.2139/ssrn.6511242.
13. Yang P, Zhang A, Bi W. Finite-time group consensus for second-order multi-agent systems with input saturation. Neural Process Lett. 2022;54(5):4211–28. doi:10.1007/s11063-022-10805-w.
14. Moradi M, Heydari M, Zarei SF. An overview on consensus-based distributed secondary control schemes in DC microgrids. Electr Power Syst Res. 2023;225(4):109870. doi:10.1016/j.epsr.2023.109870.
15. Hou Z, Zhou Z, Zhang J, Wang W, Tang Y. Self-tuning dynamic event-triggered consensus control for multi-agent systems and its implementation via self-triggering. ISA Trans. 2026;173(2):93–101. doi:10.1016/j.isatra.2026.04.006.
16. Huang B, Peng H, Ahn CK. Noncooperative game-based probability assignment formation control for networked uncrewed surface vehicles under stochastic packet losses. IEEE Trans Automat Sci Eng. 2026;23:5914–28. doi:10.1109/tase.2026.3669734.
17. Wang G, Zhang T, Jiang X, Zhang W. Event-triggered predefined-time adaptive consensus control for stochastic multi-agent systems. Nonlinear Dyn. 2026;114(8):567. doi:10.1007/s11071-026-12439-2.
18. Zhou W, Chen Z, Wang Y, Yang Y, Zhang Y. Event-triggered self-structuring neural network-based formation control of underactuated unmanned surface vessels. IEEE Trans Consumer Electron. 2026. doi:10.1109/tce.2026.3675856.
19. Li Q, Yue C. Fully distributed consensus of nonlinear fractional multi-agent systems based on combined event-triggered mechanism. Math Methods App Sci. 2026;49(3):1855–78. doi:10.1002/mma.8669.
20. Liu Y, Song W, Tong S. Observer-based cooperative fault-tolerant output regulation for Takagi–Sugeno fuzzy multi-agent systems under DoS attacks. Int J Syst Sci. 2026. doi:10.1080/00207721.2026.2634206.
21. Zhang Z, Chen S, Zheng Y. Cooperative output regulation for linear multiagent systems via distributed fixed-time event-triggered control. IEEE Trans Neural Netw Learning Syst. 2024;35(1):338–47. doi:10.1109/tnnls.2022.3174416.
22. Song L, Liang H, Ahn CK, Yang J. Event-triggered sliding mode consensus of heterogeneous agent networks: a lie-algebraic decoupling approach. IEEE Internet Things J. 2026;13(6):11983–94. doi:10.1109/jiot.2026.3656288.
23. He X, Yan Y, Li S. Adaptive fixed-time event-triggered fault-tolerant consensus for switched nonlinear multi-agent systems with actuator failures. Adapt Control Signal. 2026;40(6):1279–91. doi:10.1002/acs.70068.
24. Li S, Song C, Shi W. Dynamic event-triggered consensus control of multi-agent systems with switching topology and multiple time delays. Asian J Control. 2026;28(2):631–47. doi:10.1002/asjc.3670.
25. Hossain R, Gautam M, Olowolaju J, Livani H, Benidris M. Multi-agent voltage control in distribution systems using GAN-DRL-based approach. Electr Power Syst Res. 2024;234(1):110528. doi:10.1016/j.epsr.2024.110528.
26. Ardakan AG, Anaraki AS, Mazidi M. Multi-agent systems based on hierarchical voltage control in active low- and medium-voltage electrical distribution networks. Electr Power Syst Res. 2026;253(9):112498. doi:10.1016/j.epsr.2025.112498.
27. Jiang A, Liang D, Wang C, Tian E, Zhang J. Finite-time output regulation of singular heterogeneous linear multi-agent systems. Int J Syst Sci. 2026;57(5):1304–13. doi:10.1080/00207721.2025.2529488.
28. Dong X, Ren J. Event-triggered cooperative output regulation of switched multi-agent systems with frequent asynchronism. Adapt Control Signal. 2026;40(1):210–27. doi:10.1002/acs.4093.
29. Zhou S, Sun D, Feng G. Distributed adaptive fixed-time formation tracking for heterogeneous multi-agent systems. Automatica. 2026;183(18):112632. doi:10.1016/j.automatica.2025.112632.
30. Sun J, Li R, Yun J, Liu L, Shan Q, Zhang J. A boundary-dependent asynchronous intermittent control approach to cluster consensus of multi-agent systems. Intl J Robust Nonlinear. 2026;36(1):374–86. doi:10.1002/rnc.70141.
31. Ma H, Li L, Qu X, Ran B. Linking string stability and traffic hysteresis: implications for oscillation absorption in vehicle longitudinal control. Transp Res Part C Emerg Technol. 2026;185:105565. doi:10.1016/j.trc.2026.105565.

32. Li G, Ren CE, Chen CLP. Preview-based leader-following consensus control of distributed multi-agent systems. Inf Sci. 2021;559(1):251–69. doi:10.1016/j.ins.2020.12.081.
33. Aslam MS, Chen Z, Zhang B. Event-triggered fuzzy filtering in networked control system for a class of non-linear system with time delays. Int J Syst Sci. 2018;49(8):1587–602. doi:10.1080/00207721.2018.1463410.
34. Abbasi M, Marquez HJ. Dynamic event-triggered consensus control of multi-agent systems with time-varying delays and semi-Markovian switching topology. IEEE Trans Automat Sci Eng. 2025;22:19069–80. doi:10.1109/tase.2025.3592691.
35. Gu Z, Wu J, Zhang H, Xie X. Heterogeneous topology-based event-triggered consensus control of autonomous motorcade systems against deception attacks. IEEE Trans Veh Technol. 2025;74(4):5479–88. doi:10.1109/tvt.2024.3508253.
36. Wang K, Zhang J, Liu Y, Mu C. Cooperative control of heterogeneous connected vehicle platoons: a dynamic event-triggered reinforcement learning approach. IEEE Trans Intell Transp Syst. 2026;27(8):9901–14. doi:10.1109/tits.2026.3681134.
37. Yu J, Ma Z, Li K, Cao J. Event-driven component consensus control of connected automatic vehicles formation with DoS attacks. Nonlinear Dyn. 2025;113(20):27593–609. doi:10.1007/s11071-025-11510-8.
38. Gu Z, Yang F, Sun X. Event-triggered interval type-2 fuzzy consensus control of full-vehicle suspension systems using a leader-following approach. IEEE Trans Intell Transp Syst. 2025;26(10):16574–83. doi:10.1109/tits.2025.3581732.
39. Shen H, Wang Y, Xia J, Park JH, Wang Z. Fault-tolerant leader-following consensus for multi-agent systems subject to semi-Markov switching topologies: an event-triggered control scheme. Nonlinear Anal Hybrid Syst. 2019;34(3):92–107. doi:10.1016/j.nahs.2019.05.003.
40. Khan A, Javeed MA, Niazi AUK, Rehman S, Hassan WU, Zhong Y. A robust control framework for multi-agent systems under Byzantine attacks using hybrid event-triggered techniques. Ain Shams Eng J. 2024;15(12):103149. doi:10.1016/j.asej.2024.103149.
41. Lin YH, Chang WJ, Lee YC, Aslam MS, Ku CC. Computational design of interval type-2 fuzzy control for formation and containment of multi-agent systems with collision avoidance capability. Comput Model Eng Sci. 2025;144(2):2231–62. doi:10.32604/cmes.2025.067464.